ENERGY DEPENDENCE OF COSMIC RAYS FLUXES FOR Z=6 AND Z=8.

March 1989

Table of Contents

1.0 Energy Dependence of Cosmic Rays Fluxes for Z = 6 and Z = 8.

1.1 Abstract

The energy exponent factor of a galactic component of flux was determined for two elements, Z = 6 and Z = 8, in the energy interval of E = 50 to 150 MeV/n. The experimental events were registered by two detectors, HET-I and HET-II, of Voyager-1 and Voyager-2 satellites during the time period of minimum solar activity (12/1/77 to 4/1/78). The determined energy exponent factor of a galactic component of flux is s = 0.680 + -0.092 for Z = 6 element and s = 0.558 + /-0.116 for Z = 8. The effect of spallation process is estimated for events registered by the detector HET-II of Voyager-1. We have used two, minimum and maximum, spallation corrections. The included spallation corrections increase the energy exponent factor of flux by 1% to 13% for Z = 6 and by 2% to 22% for Z = 8 elements.

1.2 Experimental Data Analysis

We have analyzed experimental events corresponding to Z = 6 and Z = 8 during the time period of minimum solar activity (12/1/77 to 4/1/78). The data were registered by two detectors, HET-I and HET-II, on Voyager-1 and -2 satellites. The analysis is performed in two stages.

Stage 1

In the initial stage of data analysis we have determined scaling parameters (offsets and full scale MeV) of four detectors for A- and B-stopping events. The fit of scaling parameters was performed on data sets with large number of events collected in the time period of 9/18/77 to 12/26/79 (detector HET-I of Voyager-1, and detectors HET-I and HET-II of Voyager-2) and in the time period of 1/1/1986 to 12/31/1987 for HET-II of Voyager-1.

The scaling parameters are given in the Table 1 for A- and B-stopping events for both detectors, HET-I and HET-II, of Voyager-1, and -2 satellites. The experimental events and simulation tracks are shown for A- and B-stopping events for all four detectors in Figs. 1-16.

Stage 2

In the next stage of data analysis the obtained scaling parameters were used to calculate charge resolution for Z = 6 and Z = 8 elements from a small set of Voyager-1 and Voyager-2 experimental events registered in the time period of minimum solar activity of 12/1/77 to 4/1/78. The charge resolution plots are presented in Figs. 17-24 for A- and B-stopping events corresponding to Z = 6 and Z = 8 elements registered by HET-I and HET-II detectors of Voyager-I and Voyager-II satellites. To determine dependence of flux versus energy we have introduced several energy bins which limits are determined by taking into account the locations of dead layers. The ranges and energy bins for all detectors are given in the Table 2.

The experimental events, simulation tracks and marked energy bins are shown in Figs. 25 - 40 for A- and B-stopping events registered by HET-I and HET-II detectors of Voyager-I and Voyager-II satellites.

The final results of data analysis, fluxes versus energy, are presented in log-log plots (Figs 41-44 for Z = 6 and Figs 45-48 for Z = 8).

The final results also are summarized in the Table 3 which contains the energy exponent factor of a galactic component of flux for two elements, Z = 6 and Z = 8. The values in different columns correspond to HET-I and HET-II detectors of Voyager-1 and Voyager-2 satellites.

The mean value of the energy exponent factor and its error are calculated from the values given in the Table 3. The mean energy exponent factor is s = 0.680 +- 0.092 for Z = 6 and s = 0.558 +- 0.116 for Z = 8.

The effect of spallation process is calculated for events registered by HET-II of Voyager-1 (12/1/77 to 4/1/78) using two, minimum and maximum, spallation corrections. The estimated change in the energy exponent factor of flux with applied maximum spallation correction can be as large as 22% of increase for Z = 8 element and 13% of increase for Z = 6 (see Table 2).

1.3 Tables and Figures

Table 1.

Voyager-1 HET-I A stopping events

	A1	A2	C123
Offset	-3.	-3.	0.
Full Scale (MeV)	850.	850.	17300.

Voyager-1 HET-I B stopping events

	B1	B2	C432
Offset	0.	0.	0.
Full Scale (MeV)	2300.	4180.	16850.

Voyager-1 HET-II A stopping events

	A1	A2	C123
Offset	-1.	0.	0.
Full Scale (MeV)	935.	915.	17400.

Voyager-1 HET-II B stopping events

	B1	B2	C432
Offset	-1.	0.	-3.
Full Scale (MeV)	2060.	4170.	17750.

Voyager-2 HET-I A stopping events

	A1	A2	C123
Offset	0.	2.	0.
Full Scale (MeV)	890.	925.	17250.

Voyager-2 HET-I B stopping events

	B1	B2	C432
Offset	2.	3.	0.
Full Scale (MeV)	2100.	4120.	17050.

Voyager-2 HET-II A stopping events

	A1	A2	C123
Offset	-3.	0.	0.
Full Scale (MeV)	895.	860.	16600.

Voyager-2 HET-II B stopping events

	B1	B2	C432
Offset	0.	0.	0.
Full Scale (MeV)	2050.	4120.	16700.

Table 2.

Voyager-1 HET-I A stopping events

Ranges determining positions of bins

320 2200 4300 9000

Corresponding bins

Z = 6	11.26	11.78	35.65	51.96	80.32	106.43
Z = 8	13.12	13.74	41.83	61.06	94.51	125.46

Voyager-1 HET-I B stopping events

Ranges determining positions of bins

4040 5800 9300 16350

Corresponding bins

Z = 6	50.03	50.18	61.49	80.25	111.55	131.01
Z = 8	58.77	58.95	72.29	94.45	131.50	154.70

Voyager-1 HET-II A stopping events

Ranges determining positions of bins

673 1600 4179 10000

Corresponding bins

Z=6 11.30 18.19 29.78 51.14 84.47 106.43
Z=8 13.17 21.28 34.93 60.08 99.42 125.47

Voyager-1 HET-II B stopping events

Ranges determining positions of bins

5416 9100 10800 15519

Corresponding bins

Z=6 50.04 59.17 79.27 87.33 108.67 130.95
Z=8 58.77 69.56 93.30 102.83 128.04 154.62

Voyager-2 HET-I A stopping events

Ranges determining positions of bins

Z=6 320 1200 2200 4000 6800
Z=8 320 1300 2500 4200 9000

Corresponding bins

Z=6 11.05 11.78 25.31 35.64 49.89 71.20 106.38
Z=8 12.87 13.74 31.05 44.96 60.25 94.50 125.40

Voyager-2 HET-I B stopping events

Ranges determining positions of bins

4050 5400 8500 15000

Corresponding bins

Z=6 50.03 50.24 59.07 76.27 106.91 131.01
Z=8 58.77 59.03 69.43 89.75 125.92 154.70

Voyager-2 HET-II A stopping events

Ranges determining positions of bins

Z=6 320 2000 4000 6700
Z=8 320 1000 2000 4200 6700

Corresponding bins

Z=6 11.33 11.78 33.78 49.90 70.81 106.43

Z=8 13.19 13.74 26.73 39.64 60.26 83.21 125.46

Voyager-2 HET-II B stopping events

Ranges determining positions of bins

4030 5800 9400 15000

Corresponding bins

Z=6 50.03 50.24 59.07 76.27 106.91 131.01
Z=8 58.77 58.86 72.30 95.02 125.94 154.70

Table 3.

The energy exponent factor of a galactic component of flux measured in the time period of 12/1/77 to 4/1/78. We have included all events in the low gain, A- and B-stopping mode.

	Voyager-1		Voyager-2	
	HET-I	HET-II	HET-I	HET-II
Z=6	0.670+-0.161	0.781+-0.181	0.767+-0.230	0.538+-0.180
Z=8	0.666+-0.280	0.518+-0.191	0.520+-0.242	0.587+-0.239

Figure Captions

Fig.1 Fit of simulation tracks to A-stopping experimental events (Voyager-1, HET-I) registered in the time period of 9/18/77 to 12/26/79. The events are represented by energies deposited in A1 and C123 detector layers.

Fig.2 The same as in Fig.1 for the energies deposited in A2 and C123 detector layers.

Fig.3 The same as in Fig.1 for the energies deposited in B1 and C432 detector layers.

Fig.4 The same as in Fig.1 for the energies deposited in B2 and C432 detector layers.

Fig.5 Fit of simulation tracks to A-stopping experimental events (Voyager-1, HET-II) registered in the time period of 11/1/86 to 12/31/87. The events are represented by energies deposited in A1 and C123 detector layers.

Fig.6 The same as in Fig.5 for the energies deposited in A2 and C123 detector layers.

Fig.7 The same as in Fig.5 for the energies deposited in B1 and C432 detector layers.

Fig.8 The same as in Fig.5 for the energies deposited in B2 and C432 detector layers.

Fig.9 Fit of simulation tracks to A-stopping experimental events (Voyager-2, HET-I) registered in the time period of 9/18/77 to 12/26/79. The events are represented by energies deposited in A1 and C123 detector layers.

Fig.10 The same as in Fig.9 for the energies deposited in A2 and C123 detector layers.

Fig.11 The same as in Fig.9 for the energies deposited in B1 and C432 detector layers.

Fig.12 The same as in Fig.5 for the energies deposited in B2 and C432 detector layers.

Fig.13 Fit of simulation tracks to A-stopping experimental events (Voyager-2, HET-II) registered in the time period of 9/18/77 to 12/26/79. The events are represented by energies deposited in A1 and C123 detector layers.

Fig.14 The same as in Fig.13 for the energies deposited in A2 and C123 detector layers.

Fig.15 The same as in Fig.14 for the energies deposited in B1 and C432 detector layers.

Fig.16 The same as in Fig.15 for the energies deposited in B2 and C432 detector layers.

Fig.17 Number of counts versus charge Z for A-stopping events registered by Voyager-1 detector HET-I in the time period of 12/1/77 to 4/1/78.

Fig.18 Number of counts versus charge Z for B-stopping events registered by Voyager-1 detector HET-I in the time period of 12/1/77 to 4/1/78.

Fig.19 Number of counts versus charge Z for A-stopping events registered by Voyager-1 detector HET-II in the time period of 12/1/77 to 4/1/78.

Fig.20 Number of counts versus charge Z for B-stopping events registered by Voyager-1 detector HET-II in the time period of 12/1/77 to 4/1/78.

Fig.21 Number of counts versus charge Z for A-stopping events registered by Voyager-2 detector HET-I in the time period of 12/1/77 to 4/1/78.

Fig.22 Number of counts versus charge Z for B-stopping events registered by Voyager-2 detector HET-I in the time period of 12/1/77 to 4/1/78.

Fig.23 Number of counts versus charge Z for A-stopping events registered by Voyager-2 detector HET-II in the time period of 12/1/77 to 4/1/78.

Fig.24 Number of counts versus charge Z for B-stopping events registered by Voyager-2 detector HET-II in the time period of 12/1/77 to 4/1/78.

Fig.25 Fit of simulation tracks to A-stopping experimental events (Voyager-1, HET-I) registered in the time period of 12/1/77 to 4/1/78. The events are represented by energies deposited in A1 and C123 detector layers.

Fig.26 The same as in Fig.25 for the energies deposited in A2 and C123 detector layers.

Fig.27 The same as in Fig.25 for the energies deposited in B1 and C432 detector layers.

Fig.28 The same as in Fig.25 for the energies deposited in B2 and C432 detector layers.

Fig.29 Fit of simulation tracks to A-stopping experimental events (Voyager-1, HET-II) registered in the time period of 12/1/77 to 4/1/78. The events are represented by energies deposited in A1 and C123 detector layers.

Fig.30 The same as in Fig.29 for the energies deposited in A2 and C123 detector layers.

Fig.31 The same as in Fig.29 for the energies deposited in B1 and C432 detector layers.

Fig.32 The same as in Fig.29 for the energies deposited in B2 and C432 detector layers.

Fig.33 Fit of simulation tracks to A-stopping experimental events (Voyager-2, HET-I) registered in the time period of 12/1/77 to 4/1/78. The events are represented by energies deposited in A1 and C123 detector layers.

Fig.34 The same as in Fig.33 for the energies deposited in A2 and C123 detector layers.

Fig.35 The same as in Fig.33 for the energies deposited in B1 and C432 detector layers.

Fig.36 The same as in Fig.33 for the energies deposited in B2 and C432 detector layers.

Fig.37 Fit of simulation tracks to A-stopping experimental events (Voyager-2, HET-II) registered in the time period of 12/1/77 to 4/1/78. The events are represented by energies deposited in A1 and C123 detector layers.

Fig.38 The same as in Fig.37 for the energies deposited in A2 and C123 detector layers.

Fig.39 The same as in Fig.37 for the energies deposited in B1 and C432 detector layers.

Fig.40 The same as in Fig.37 for the energies deposited in B2 and C432 detector layers.

Fig.41 Flux versus energy (log-log scale) for $Z=6$. The values of flux presented in figure are obtained from the analysis of both A- and B-stopping events registered by Voyager-1 detector HET-I in the time period of 12/01/77 - 4/01/78.

Fig.42 Flux versus energy (log-log scale) for $Z=6$. The values of flux presented in figure are obtained from the analysis of both A- and B-stopping events registered by Voyager-1 detector HET-II in the time period of 12/01/77 - 4/01/78.

Fig.43 Flux versus energy (log-log scale) for $Z=6$. The values of flux presented in figure are obtained from the analysis of both A- and B-stopping events registered by Voyager-2 detector HET-I in the time period of 12/01/77 - 4/01/78.

Fig.44 Flux versus energy (log-log scale) for $Z=6$. The values of flux presented in figure are obtained from the analysis of both A- and B-stopping events registered by Voyager-2 detector HET-II in the time period of 12/01/77 - 4/01/78.

Fig.45 Flux versus energy (log-log scale) for $Z=8$. The values of flux presented in figure are obtained from the analysis of both A- and B-stopping events registered by Voyager-1 detector HET-I in the time period of 12/01/77 - 4/01/78.

Fig.46 Flux versus energy (log-log scale) for $Z=8$. The values of flux presented in figure are obtained from the analysis of both A- and B-stopping events registered by Voyager-1 detector HET-II in the time period of 12/01/77 - 4/01/78.

Fig.47 Flux versus energy (log-log scale) for $Z=8$. The values of flux presented in figure are obtained from the analysis of both A- and B-stopping events registered by Voyager-2 detector HET-I in the time period of 12/01/77 - 4/01/78.

Fig.48 Flux versus energy (log-log scale) for $Z=8$. The values of flux presented in figure are obtained from the analysis of both A- and B-stopping events registered by Voyager-2 detector HET-II in the time period of 12/01/77 - 4/01/78.

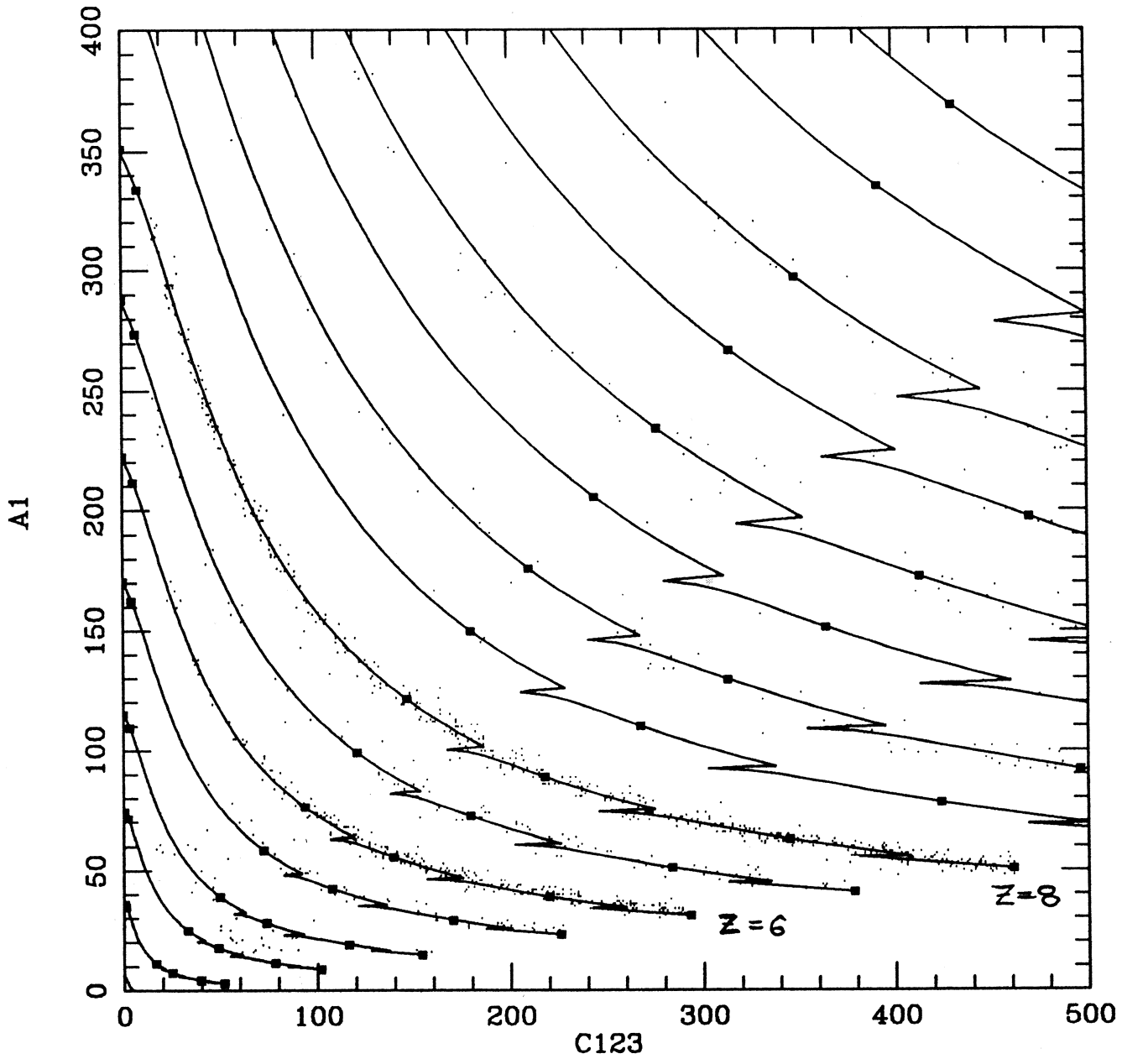

data file: s3v11a7_9.dat

evts read and selected: 1813 1615

|z2−z1| < 3.00*sigma, with sigma = 0.0550 + 0.0055*z

Energy bins from: ebv11a.dat

simulation file: trv1h1.sim

Offset D1, D2, C: −3.00 −3.00 0.00

FSMeV D1, D2, C: 850. 850. 17300.

Voyager-1

HET-I

9/18/77 - 12/26/79

Low Gain events

Fig.1 Fit of simulation tracks to A-stopping experimental events (Voyager-1, HET-I) registered in the time period of 9/18/77 to 12/26/79. The events are represented by energies deposited in A1 and C123 detector layers.

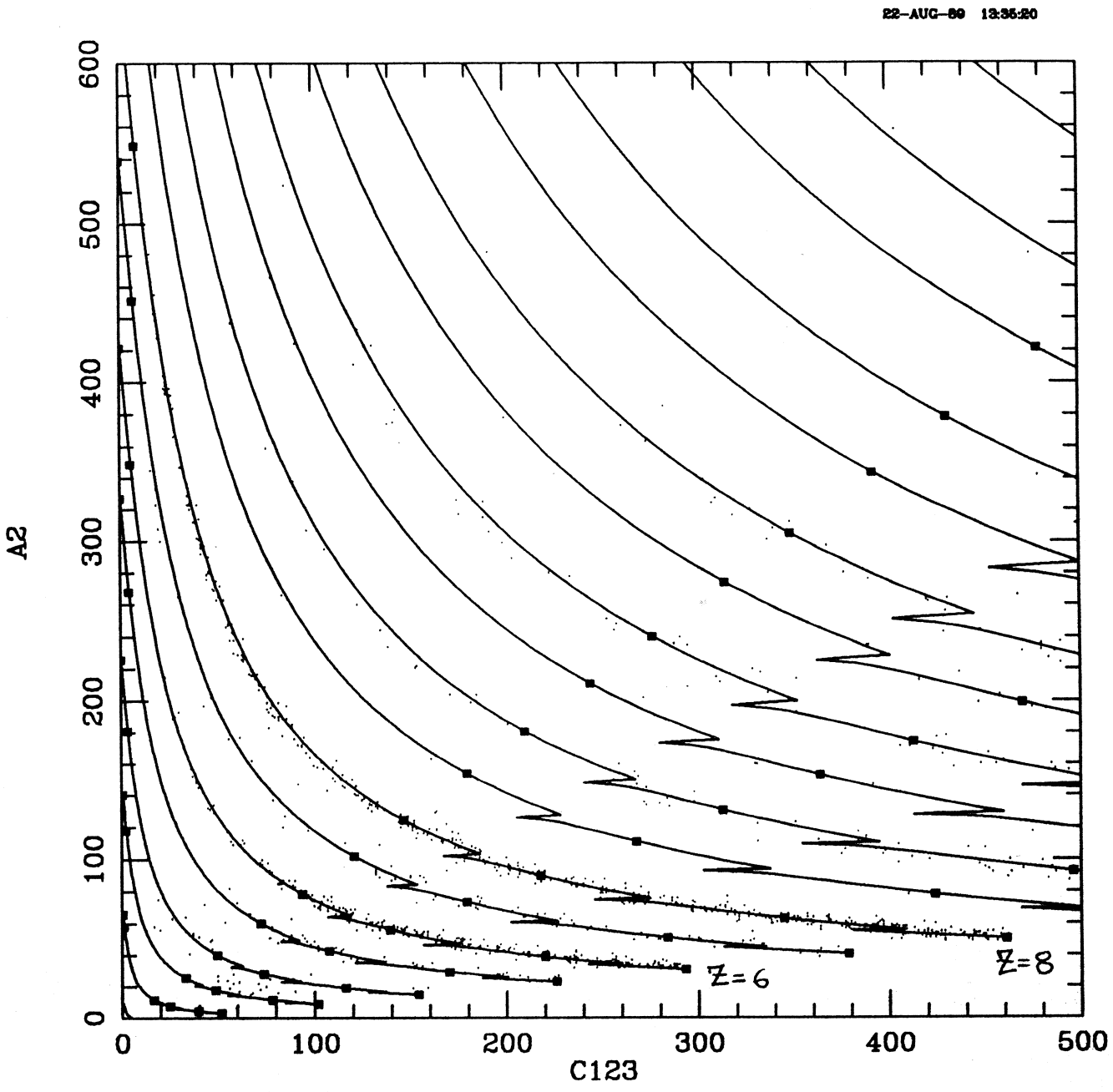

data file: s3v11a7_9.dat

evts read and selected: 1813 1615

|z2−z1| < 3.00*sigma, with sigma = 0.0550 + 0.0055*z

Energy bins from: ebv11a.dat

simulation file: trv1h1.sim

Offset D1, D2, C: −3.00 −3.00 0.00

FSMeV D1, D2, C: 850. 850. 17300.

Voyager-1, HET-I

9/18/77 - 12/26/79

Low Gain events

Fig.2 The same as in Fig.1 for the energies deposited in A2 and C123 detector layers.

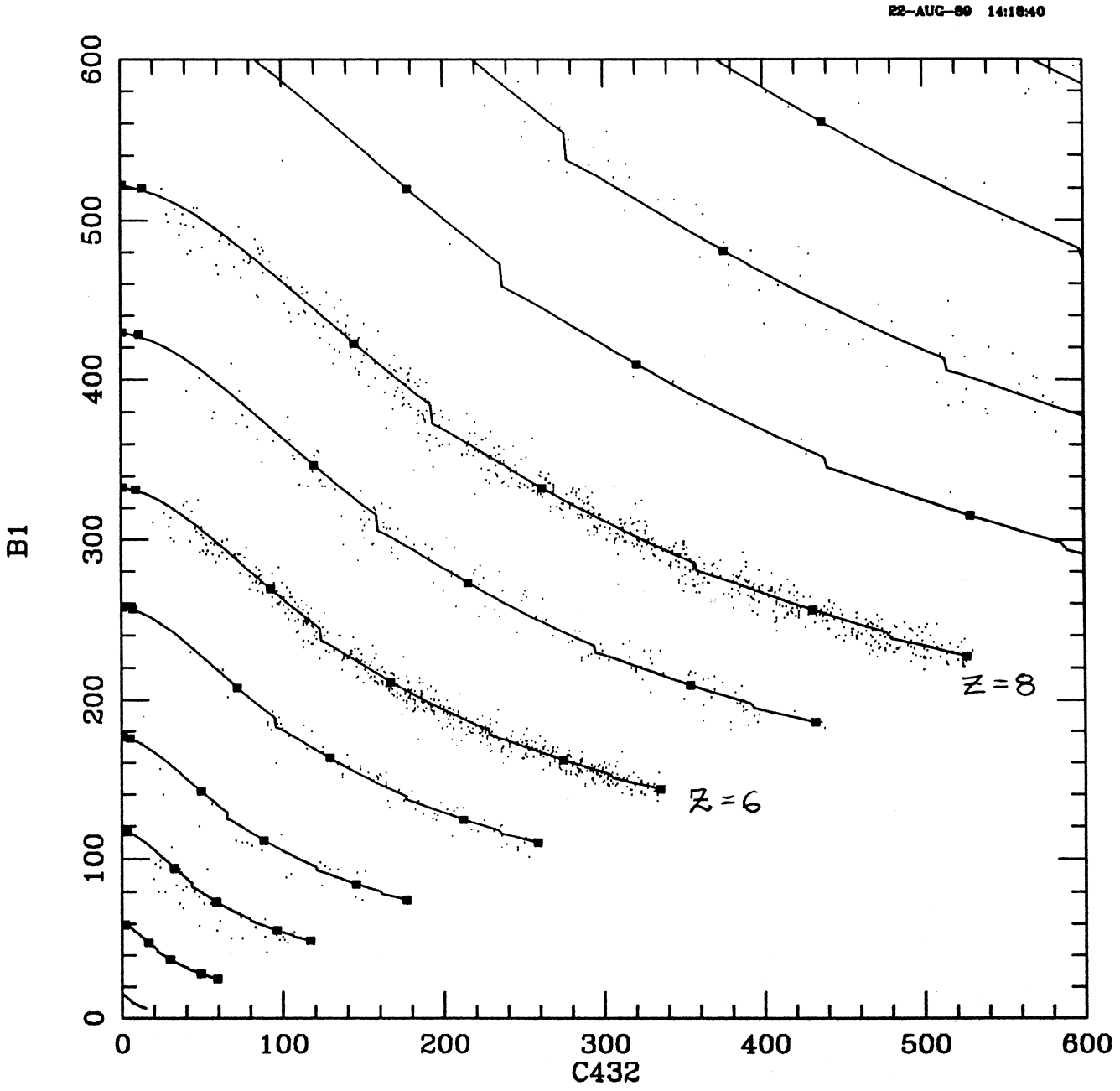

data file: s3v11b7_9.dat

evts read and selected: 2618 2214

|z2−z1| < 3.00*sigma, with sigma = 0.0550 + 0.0055*z

Energy bins from: ebv11b.dat

simulation file: trv1h1.sim

Offset D1, D2, C: 0.00 0.00 0.00

FSMeV D1, D2, C: 2300. 4180. 16850.

Voyager-1, HET-I

9/18/77 - 12/26/79

Low Gain mode

Fig.3 The same as in Fig.1 for the energies deposited in B1 and C432 detector layers.

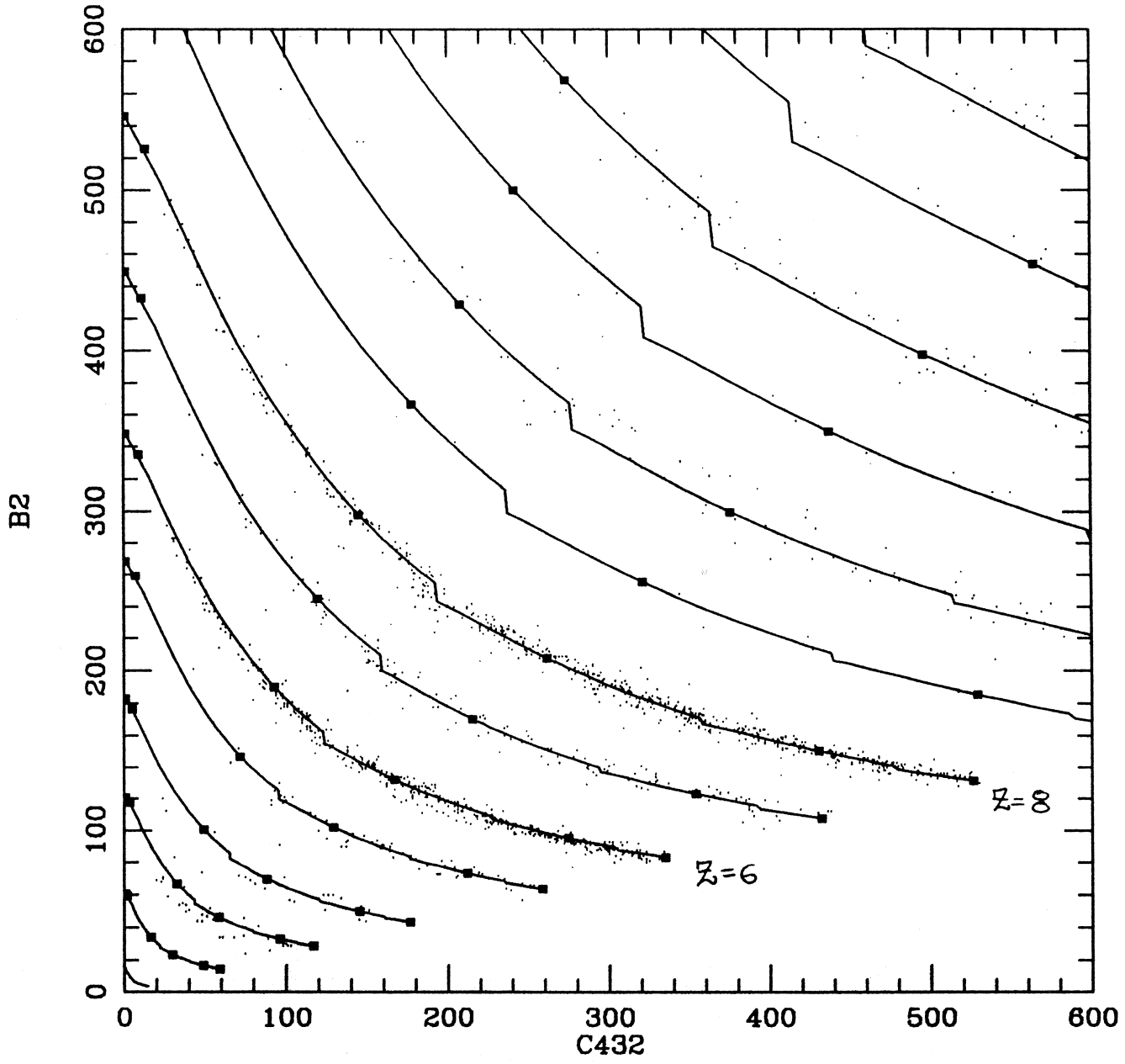

data file: s3v11b7_9.dat

evts read and selected: 2618 2214

|z2−z1| < 3.00*sigma, with sigma = 0.0550 + 0.0055*z

Energy bins from: ebv11b.dat

simulation file: trv1h1.sim

Offset D1, D2, C: 0.00 0.00 0.00

FSMeV D1, D2, C: 2300. 4180. 16850.

Voyager-1, HET-I

9/18/77-12/26/79

Low Gain mod

Fig.4 The same as in Fig.1 for the energies deposited in B2 and C432 detector layers.

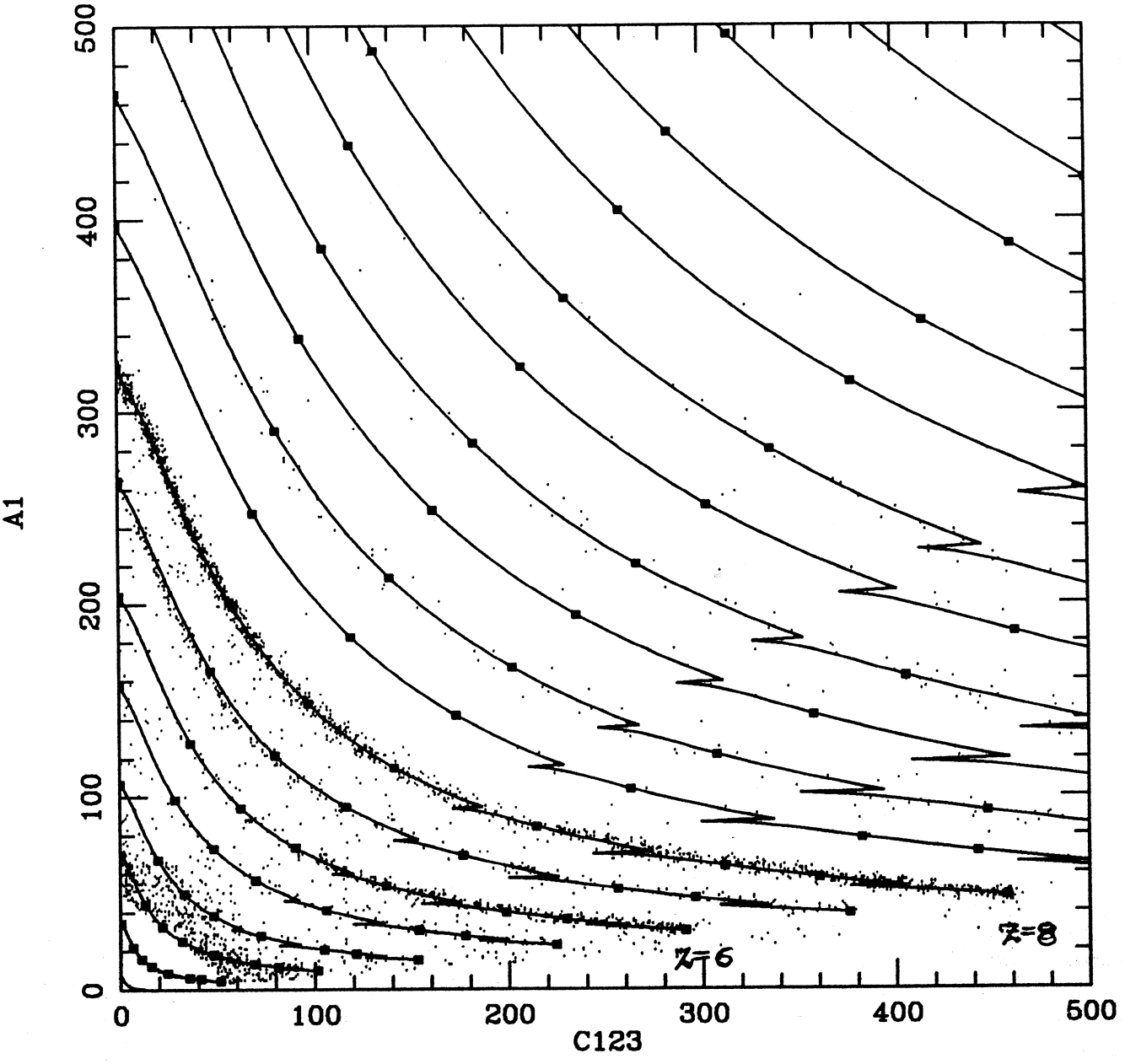

data file: lv1ast8687.dat

evts read and selected: 4079 4079

No selection on charge consistency

Energy bins from: binsv1as.dat

simulation file: repv1dl1.sim

Offset D1, D2, C: −1.00 0.00 0.00

FSMeV D1, D2, C: 935. 915. 17400.

Voyager-1, HET-II
Low Gain Mode

Fig.5 Fit of simulation tracks to A-stopping experimental events (Voyager-1, HET-II) registered in the time period of 11/1/86 to 12/31/87. The events are represented by energies deposited in A1 and C123 detector layers.

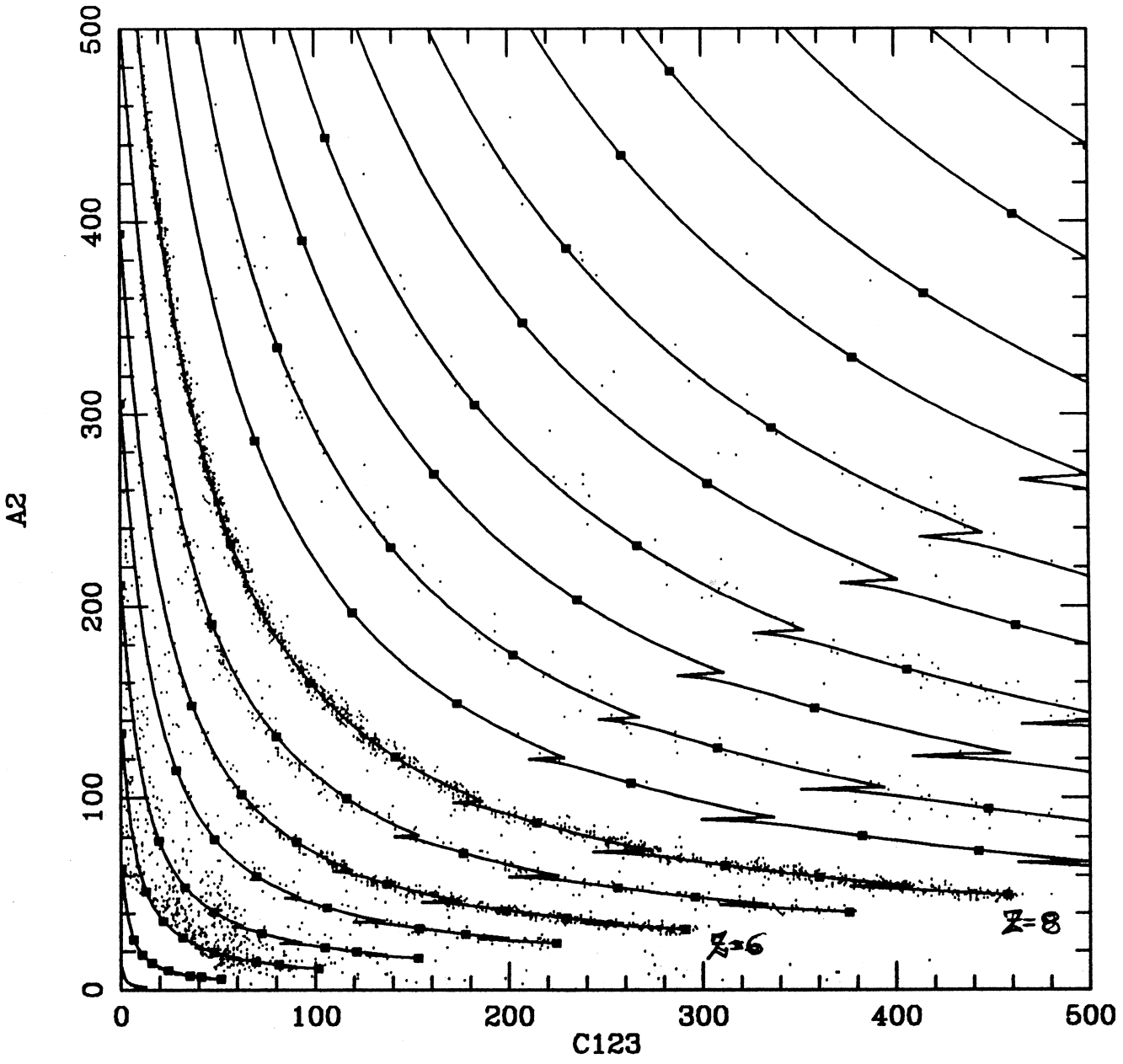

data file: lv1ast8687.dat

Voyager-1 , HET-II

# evts read and selected:	4079	4079	11/1/86 - 12/31/87

No selection on charge consistency

Energy bins from: binsv1as.dat

simulation file: repv1dl1.sim

Offset D1, D2, C:	−1.00	0.00	0.00
FSMeV D1, D2, C:	935.	915.	17400.

Fig.6 The same as in Fig.5 for the energies deposited in A2 and C123 detector layers.

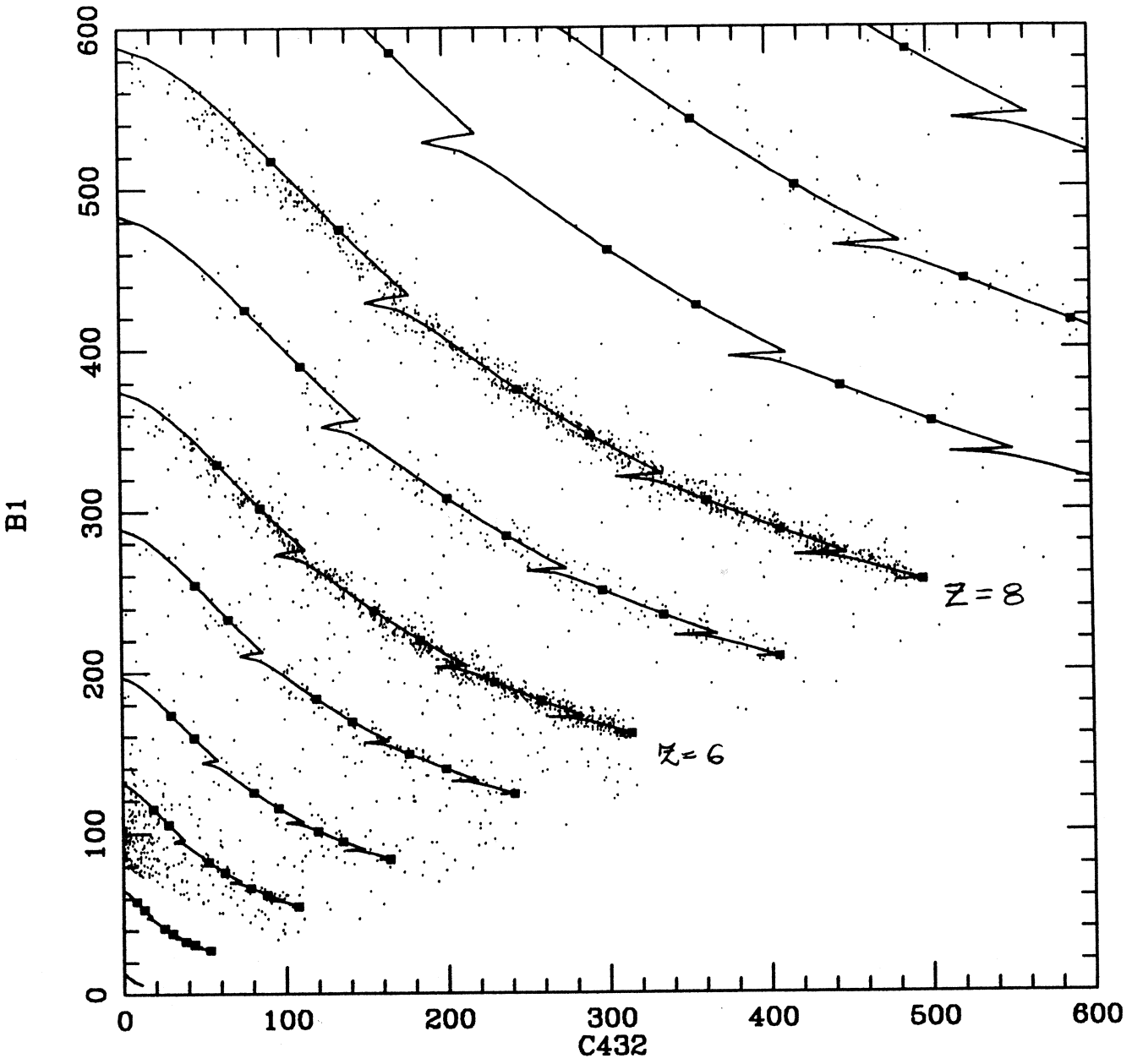

data file: lv1bst8687.dat

Voyager-1, HET-II

evts read and selected: 3738 3738

12/1/86 - 12/31/87

No selection on charge consistency

Energy bins from: binsv1bs.dat

simulation file: repv1dl1.sim

Offset D1, D2, C:	−1.00	0.00	−3.00
FSMeV D1, D2, C:	2060.	4170.	17750.

Fig.7 The same as in Fig.5 for the energies deposited in B1 and C432 detector layers.

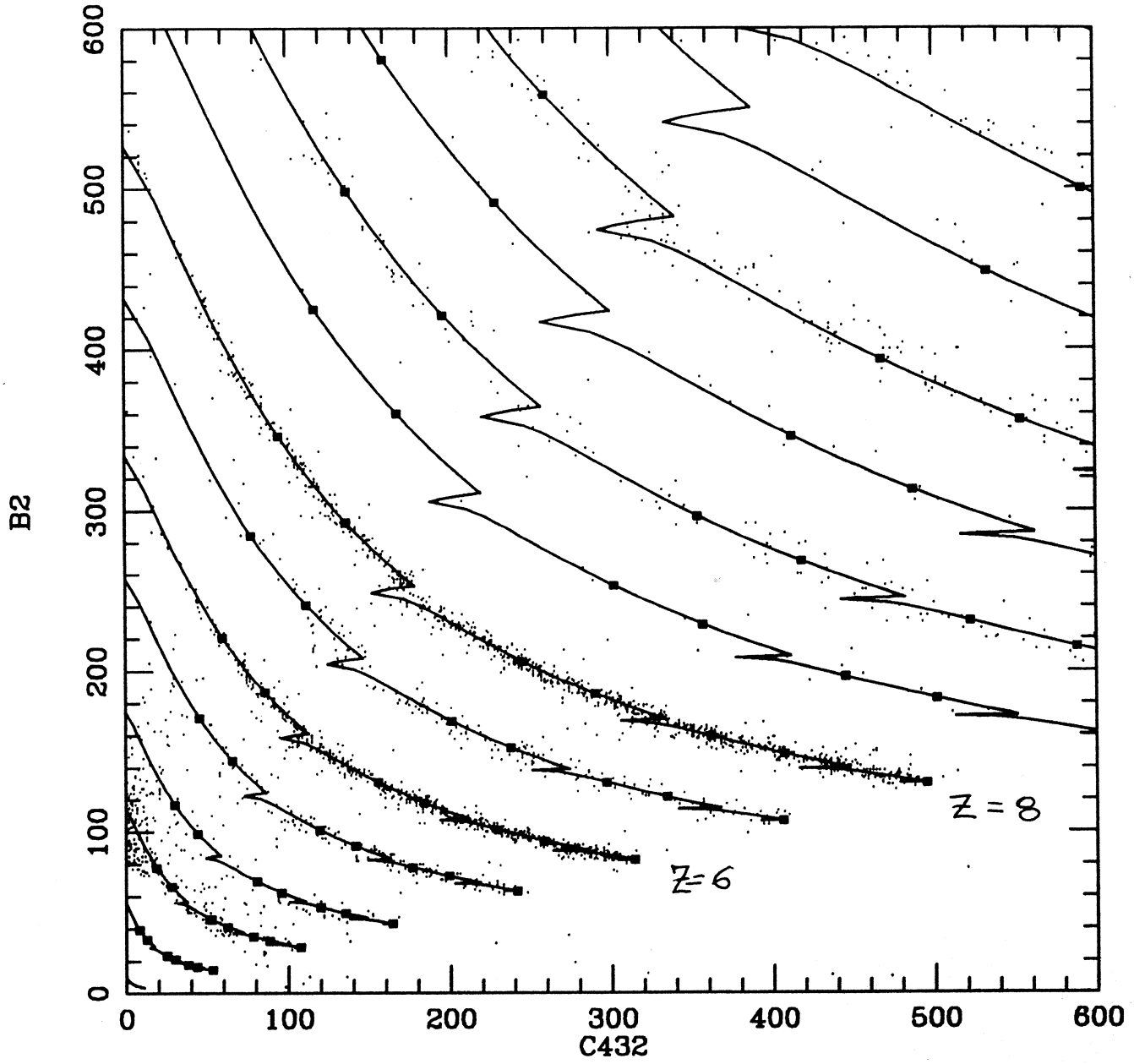

data file: lv1bst8687.dat

evts read and selected: 3738 3738

No selection on charge consistency

Energy bins from: binsv1bs.dat

simulation file: repv1dl1.sim

Offset D1, D2, C: −1.00 0.00 −3.00

FSMeV D1, D2, C: 2060. 4170. 17750.

Voyager-1, HET-II

12/1/86 - 12/31/87

Fig.8 The same as in Fig.5 for the energies deposited in B2 and C432 detector layers.

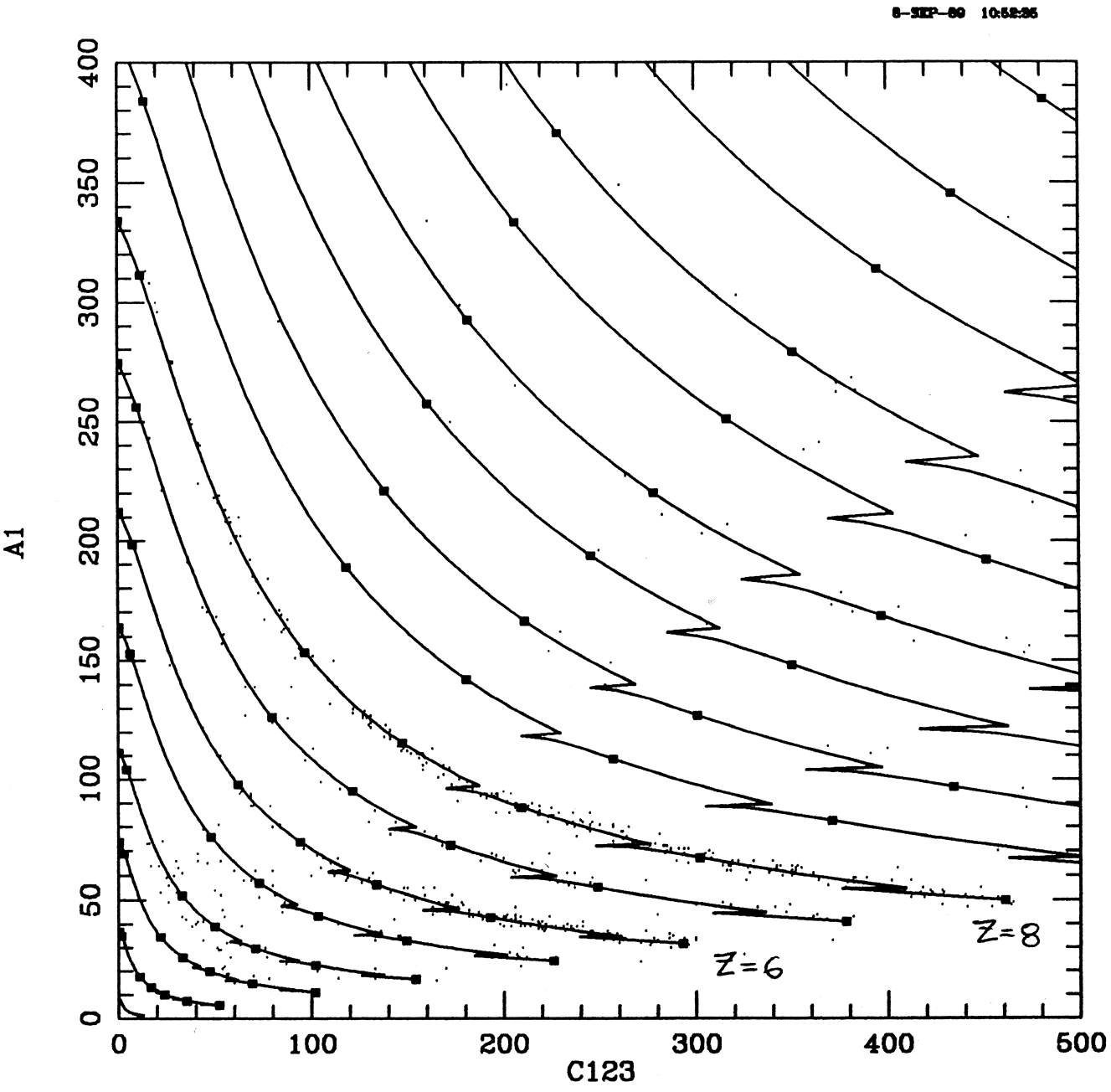

data file: s4v21a7_9.dat

evts read and selected: 799 799

No selection on charge consistency

Energy bins from: ebz6v21a.dat

simulation file: trv2h1.sim

Offset D1, D2, C: 0.00 2.00 0.00

FSMeV D1, D2, C: 890. 925. 17250.

Voyager-2, HET-I

9/18/77 - 12/26/79

Fig.9 Fit of simulation tracks to A-stopping experimental events (Voyager-2, HET-I) registered in the time period of 9/18/77 to 12/26/79. The events are represented by energies deposited in A1 and C123 detector layers.

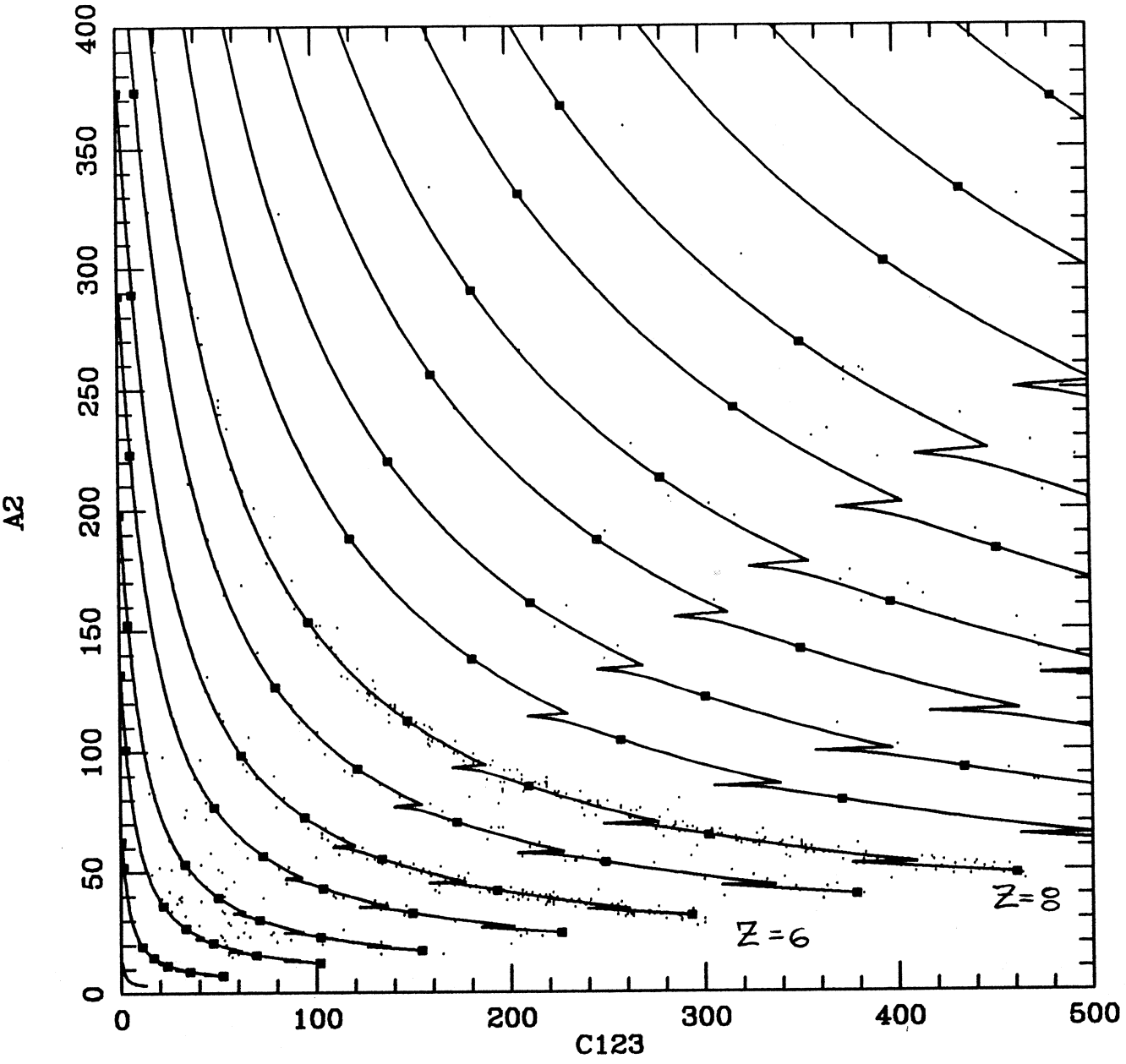

data file: s4v21a7_9.dat

evts read and selected: 799 799

No selection on charge consistency

Energy bins from: ebz6v21a.dat

simulation file: trv2h1.sim

Offset D1, D2, C: 0.00 2.00 0.00

FSMeV D1, D2, C: 890. 925. 17250.

Voyager-2, HET-I

9/18/77 - 12/26/79

Fig.10 The same as in Fig.9 for the energies deposited in A2 and C123 detector layers.

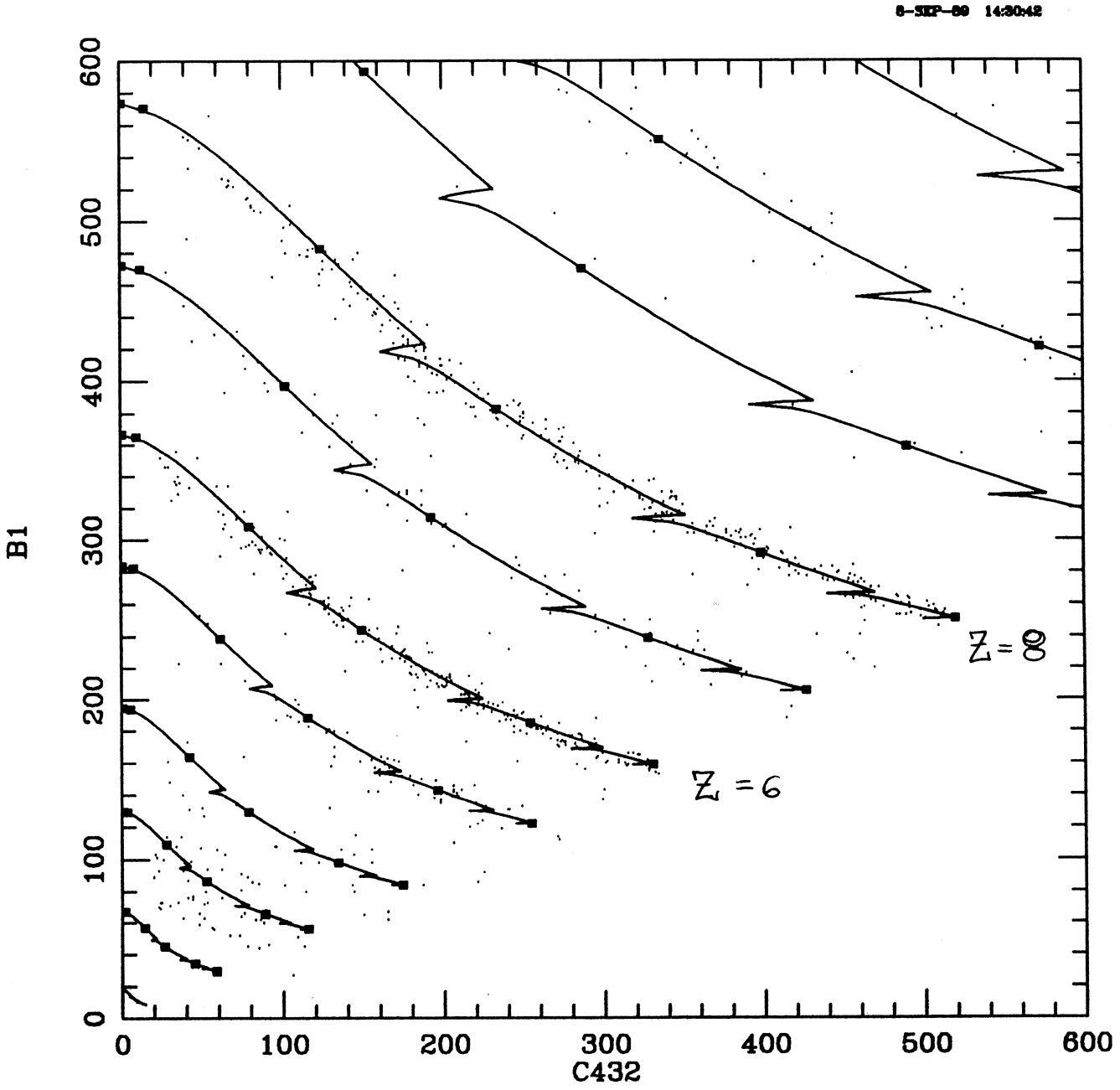

data file: s4v21b7_9.dat

evts read and selected: 1245 1245

No selection on charge consistency

Energy bins from: ebz8v21b.dat

simulation file: trv2h1.sim

Offset D1, D2, C: 2.00 3.00 0.00

FSMeV D1, D2, C: 2100. 4120. 17050.

Voyager-2, HET-I

9/18/77 - 12/26/79

Fig.11 The same as in Fig.9 for the energies deposited in B1 and C432 detector layers.

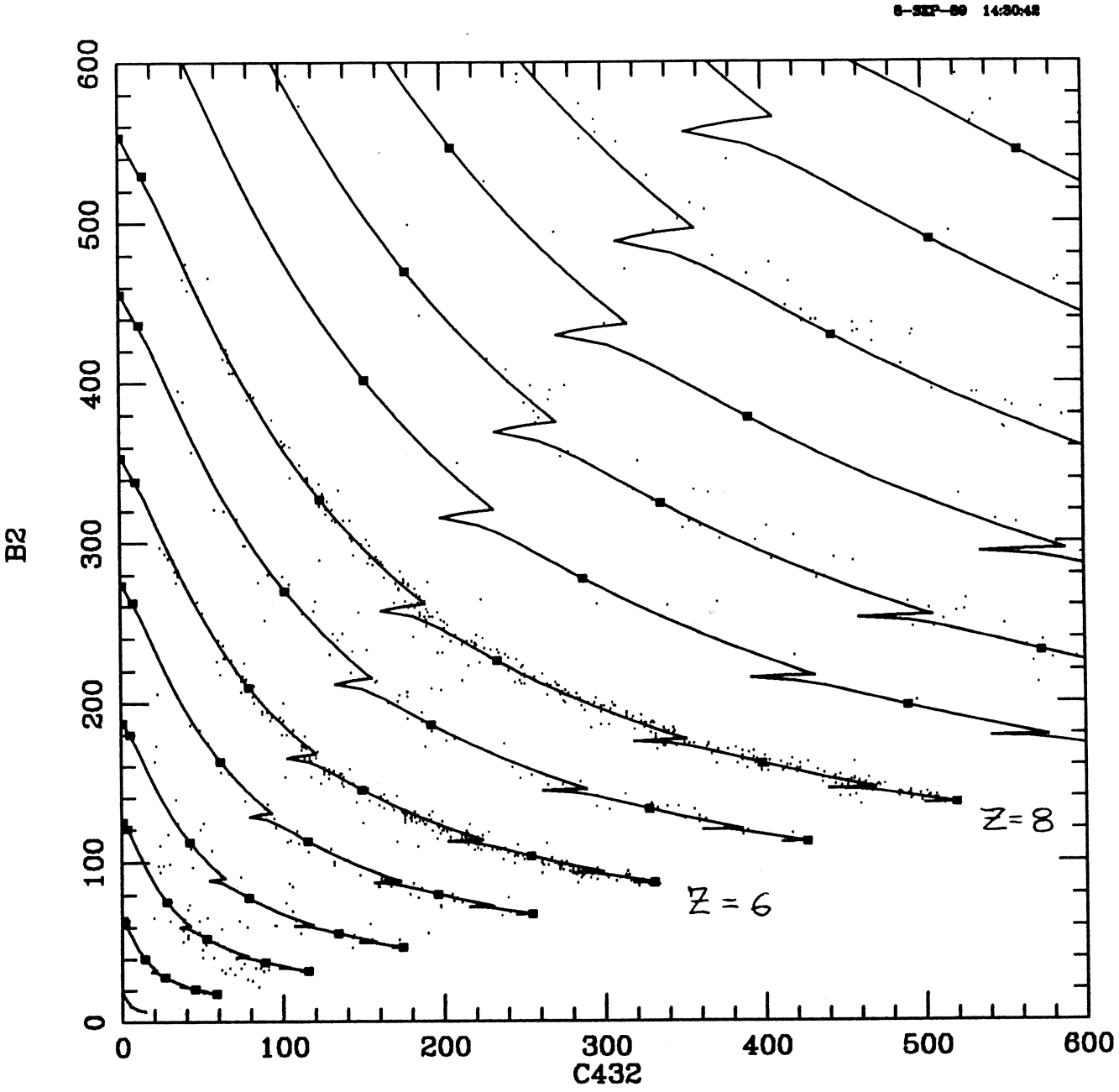

Voyager-2, HET-I
9/18/77 - 12/26/79

data file: s4v21b7_9.dat

evts read and selected: 1245 1245

No selection on charge consistency

Energy bins from: ebz8v21b.dat

simulation file: trv2h1.sim

Offset D1, D2, C: 2.00 3.00 0.00

FSMeV D1, D2, C: 2100. 4120. 17050.

Fig.12 The same as in Fig.5 for the energies deposited in B2 and C432 detector layers.

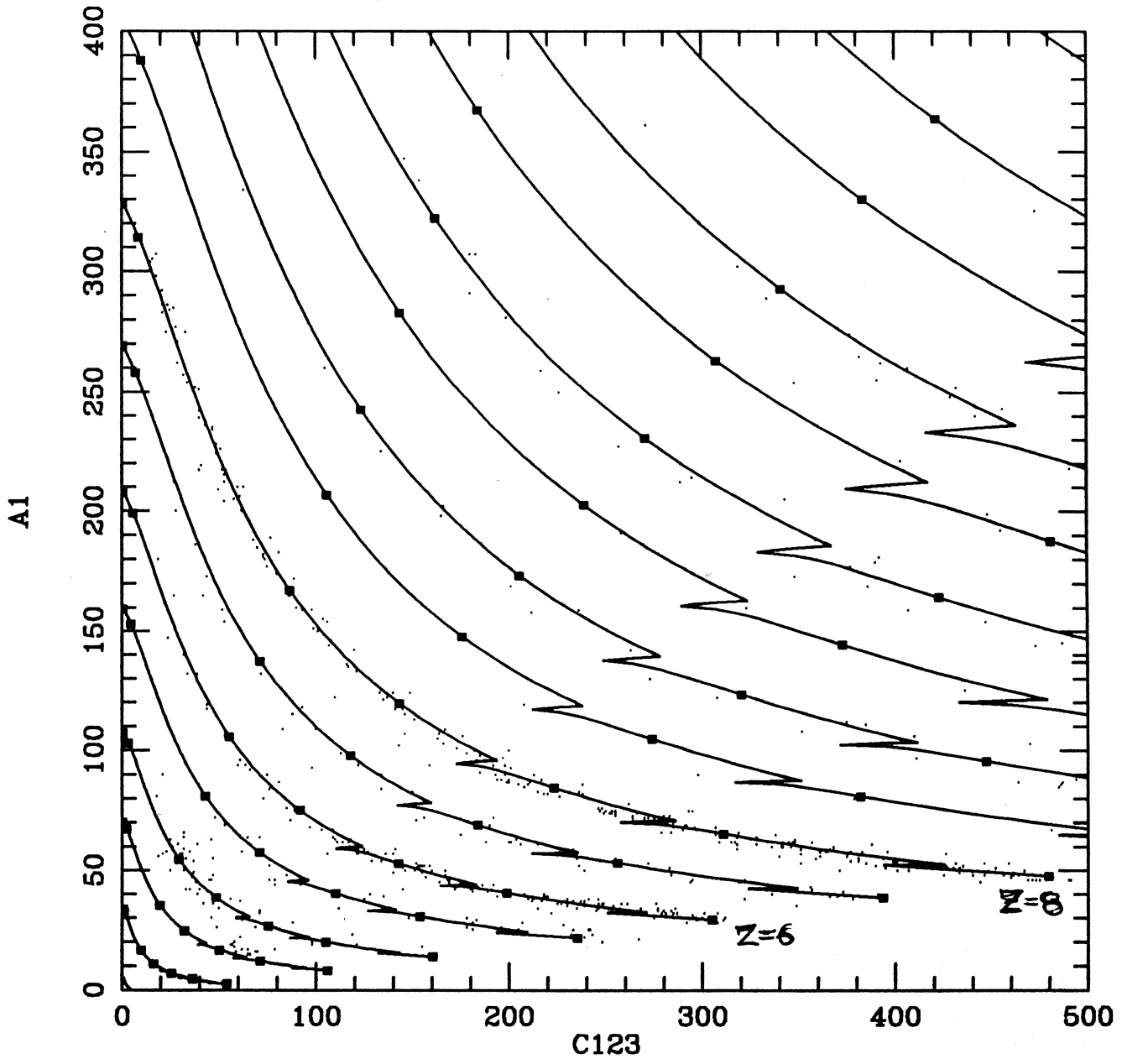

data file: s3v22a7_9.dat

evts read and selected: 940 940

No selection on charge consistency

Energy bins from: ebinv22a.dat

simulation file: trv2h2.sim

Offset D1, D2, C: −3.00 0.00 0.00

FSMeV D1, D2, C: 895. 860. 16600.

Voyager-2, HET-II
9/18/77 – 12/26/79

Fig.13 Fit of simulation tracks to A-stopping experimental events (Voyager-2, HET-II) registered in the time period of 9/18/77 to 12/26/79. The events are represented by energies deposited in A1 and C123 detector layers.

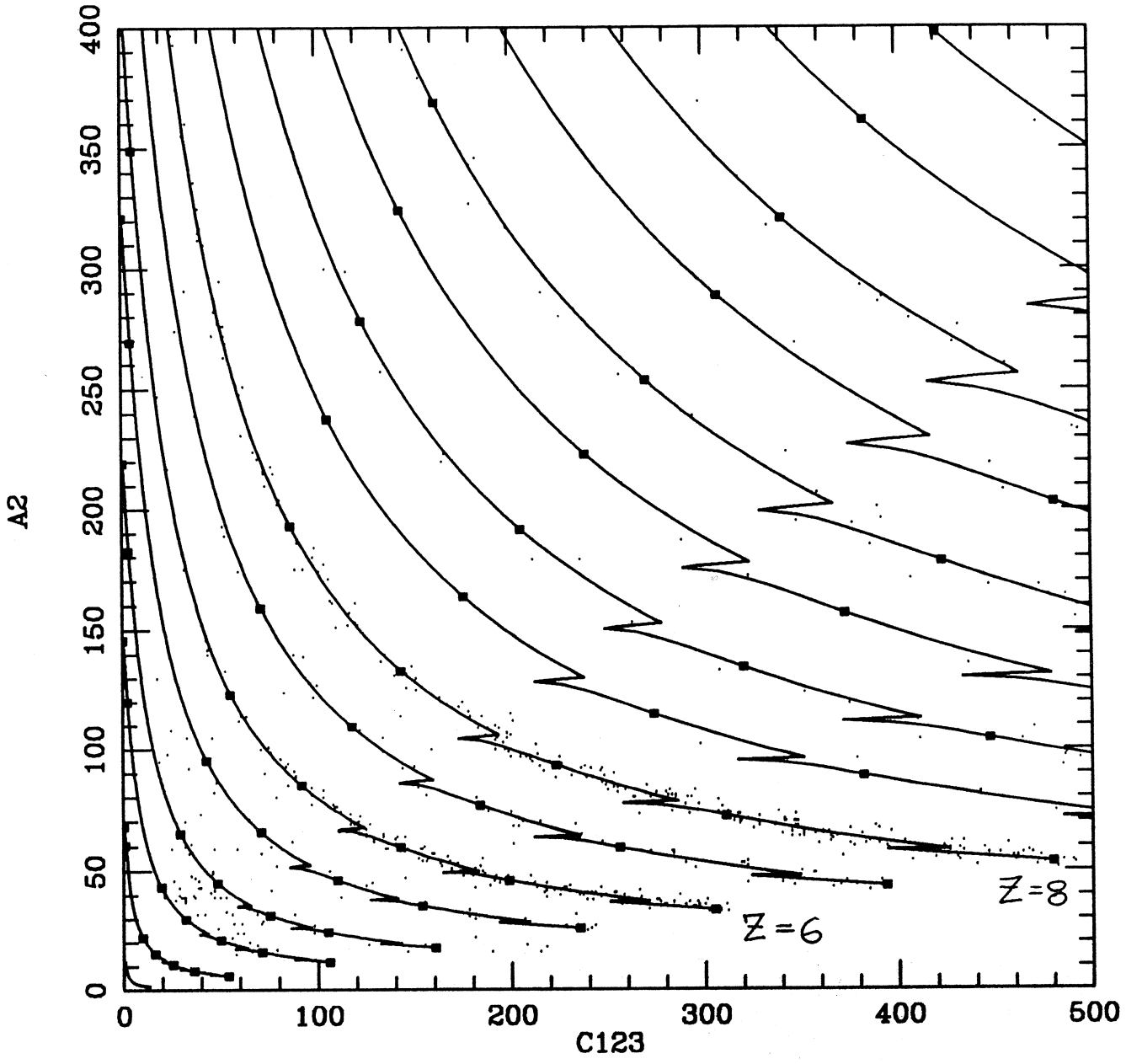

data file: s3v22a7_9.dat

evts read and selected: 940 940

No selection on charge consistency

Energy bins from: ebinv22a.dat

simulation file: trv2h2.sim

Offset D1, D2, C: −3.00 0.00 0.00

FSMeV D1, D2, C: 895. 860. 16600.

Voyager-2, HET-II
9/18/77 - 12/26/79

Fig.14 The same as in Fig.13 for the energies deposited in A2 and C123 detector layers.

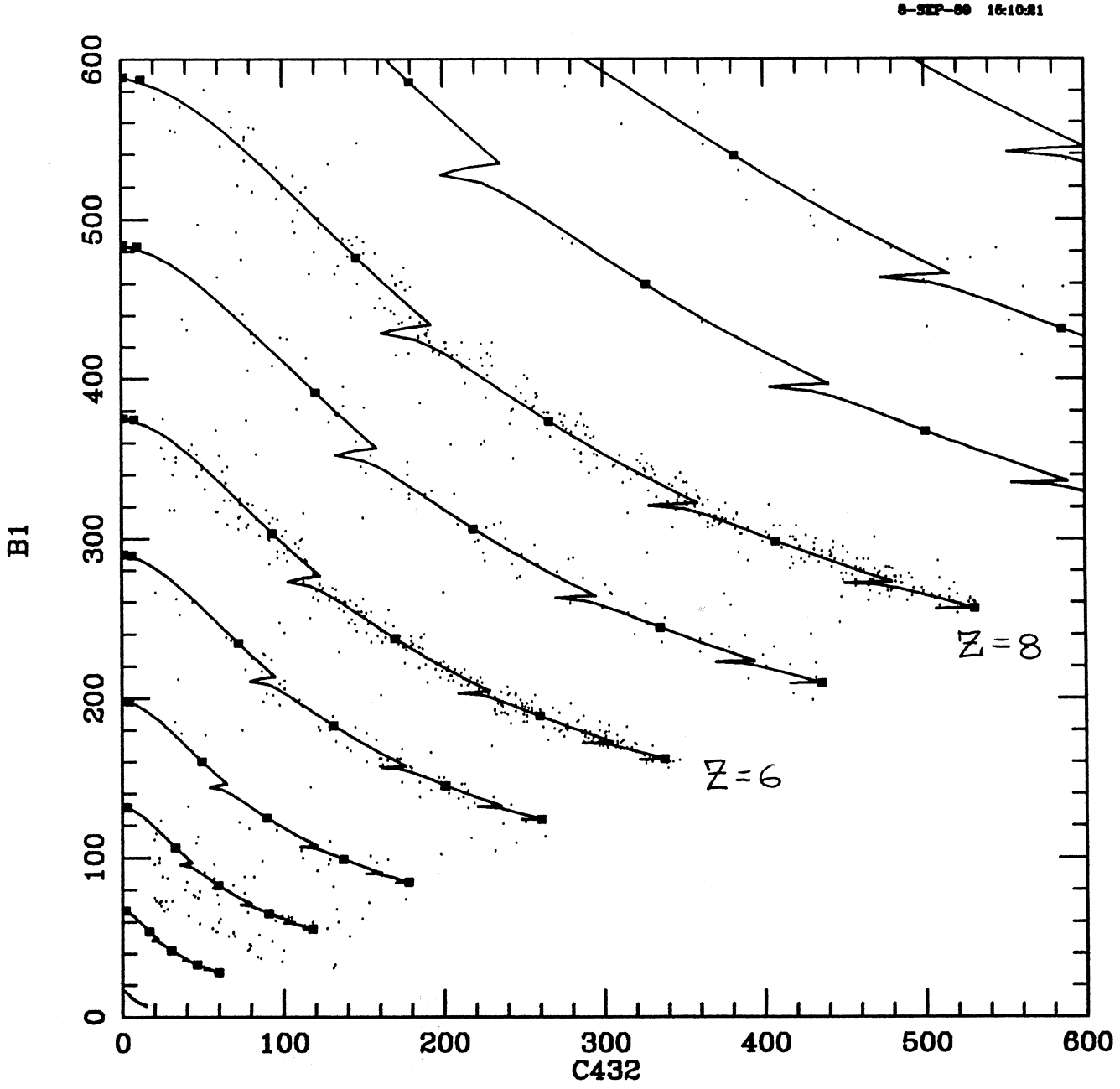

data file: s3v22b7_9.dat

evts read and selected: 1264 1264

No selection on charge consistency

Energy bins from: ebinv22b.dat

simulation file: trv2h2.sim

Offset D1, D2, C: 0.00 0.00 0.00

FSMeV D1, D2, C: 2050. 4120. 16700.

Voyager-2, HET-II

9/18/77-12/26/79

Fig.15 The same as in Fig.14 for the energies deposited in B1 and C432 detector layers.

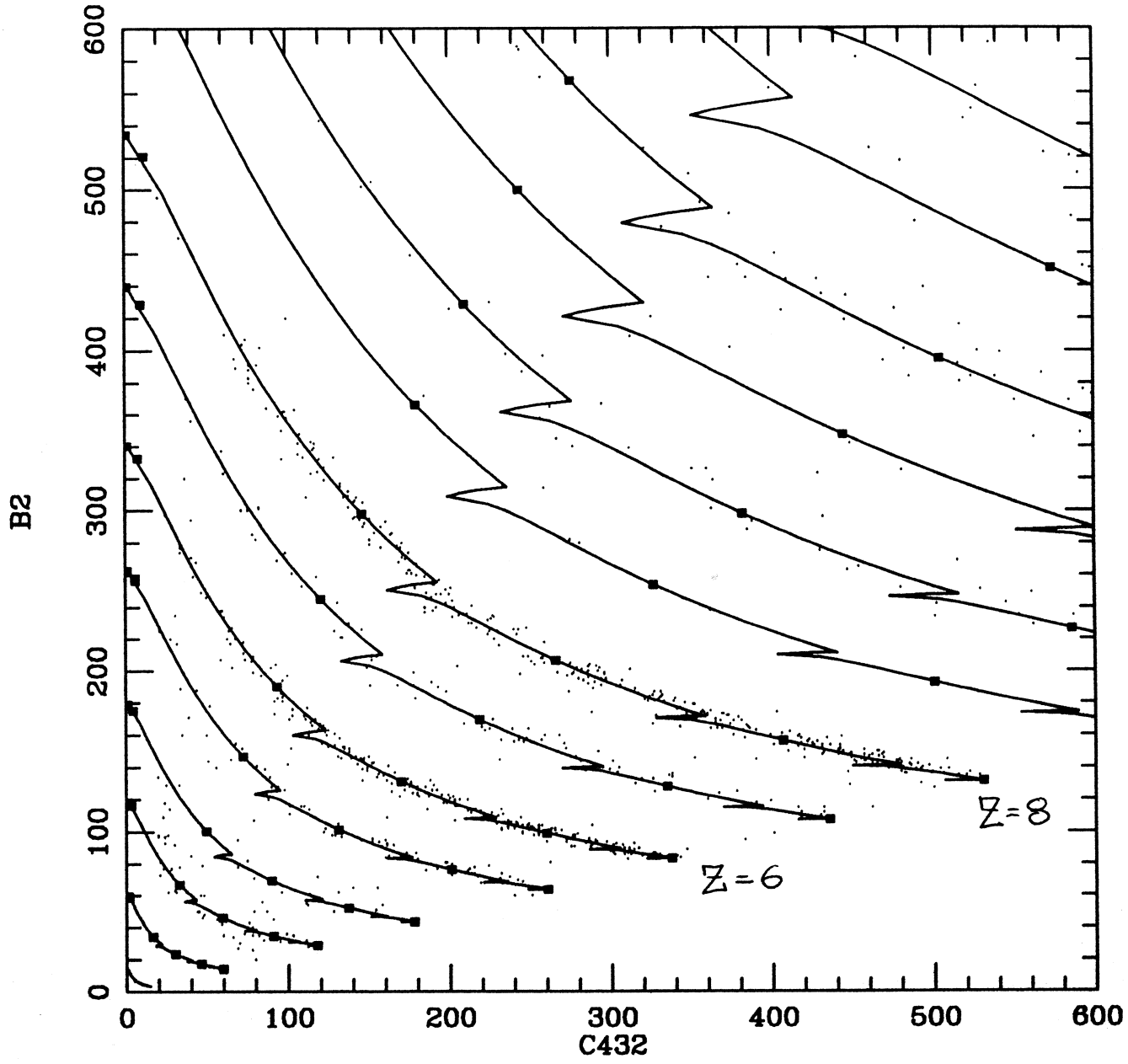

data file: s3v22b7_9.dat

evts read and selected: 1264 1264

No selection on charge consistency

Energy bins from: ebinv22b.dat

simulation file: trv2h2.sim

Offset D1, D2, C: 0.00 0.00 0.00

FSMeV D1, D2, C: 2050. 4120. 16700.

Voyager-2, HET-II

9/18/77 - 12/26/79

Fig.16 The same as in Fig.15 for the energies deposited in B2 and C432 detector layers.

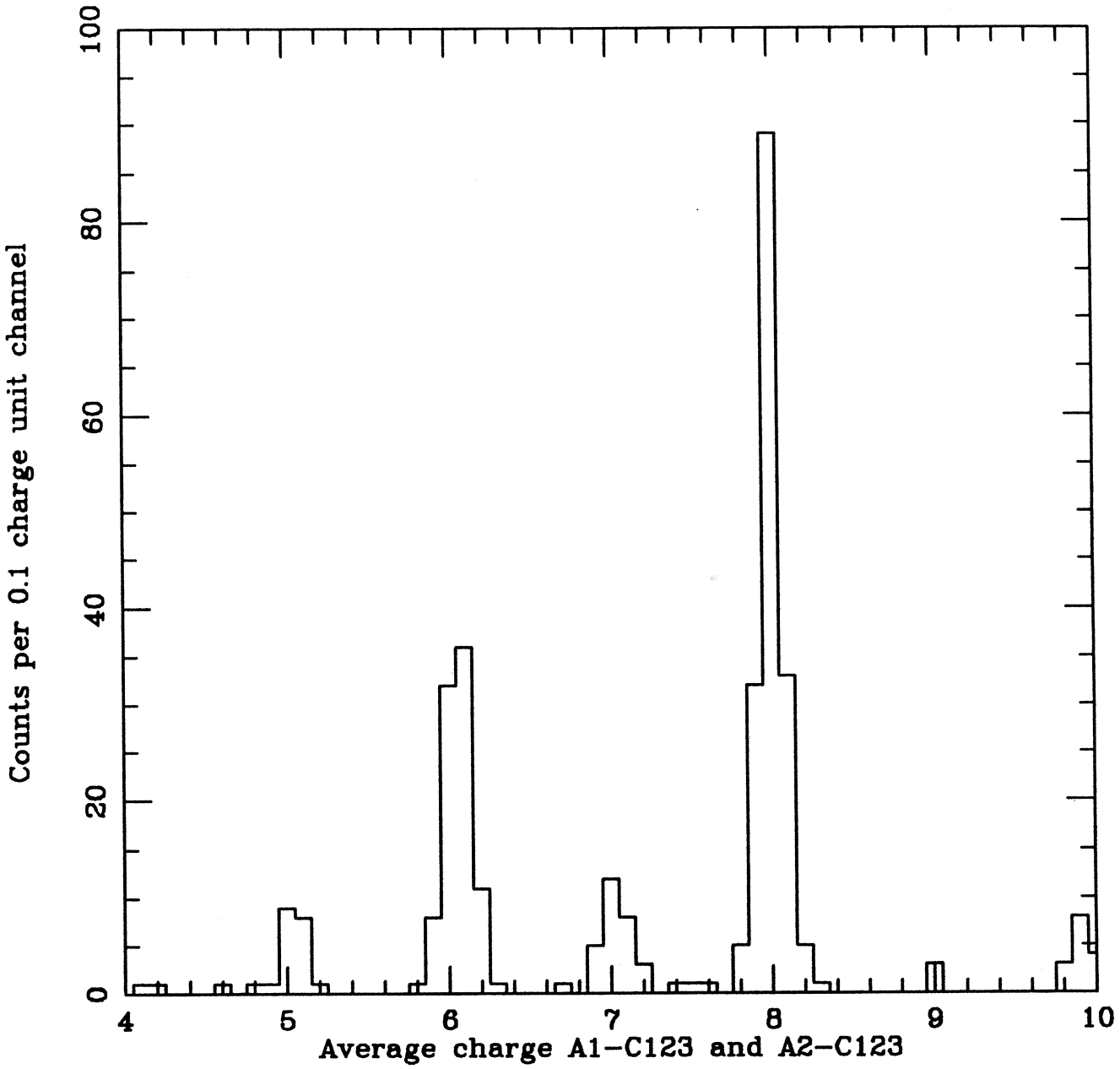

data file: S3V11A7_8.DAT

 # evts read: 490

444evts selected with |Z2-Z1| < 3.00 sigma

sigma = 0.0550 + 0.0055*zav

Voyager-1, HET-I

12/1/77 - 4/1/78

Low Gain

A-stopping events

Fig.17 Number of counts versus charge Z for A-stopping events registered by Voyager-1 detector HET-I in the time period of 12/1/77 to 4/1/78.

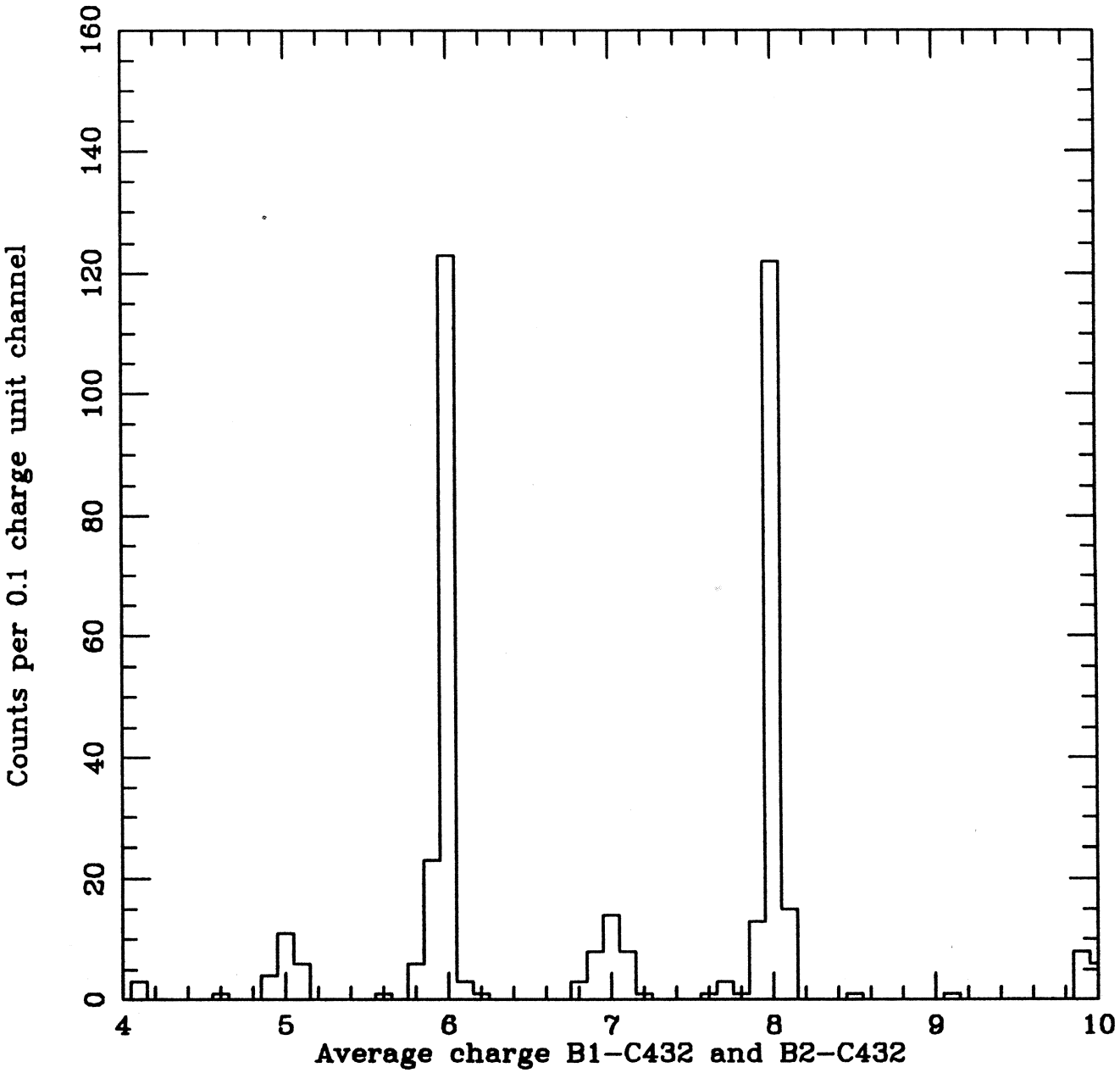

data file: S3V11B7_8.DAT

 # evts read: 655

553evts selected with |Z2-Z1| < 3.00 sigma

sigma = 0.0550 + 0.0055*zav

Voyager-1, HET-I

12/1/77 - 4/1/78

Low Gain

B-stopping events

Fig.18 Number of counts versus charge Z for B-stopping events registered by Voyager-1 detector HET-I in the time period of 12/1/77 to 4/1/78.

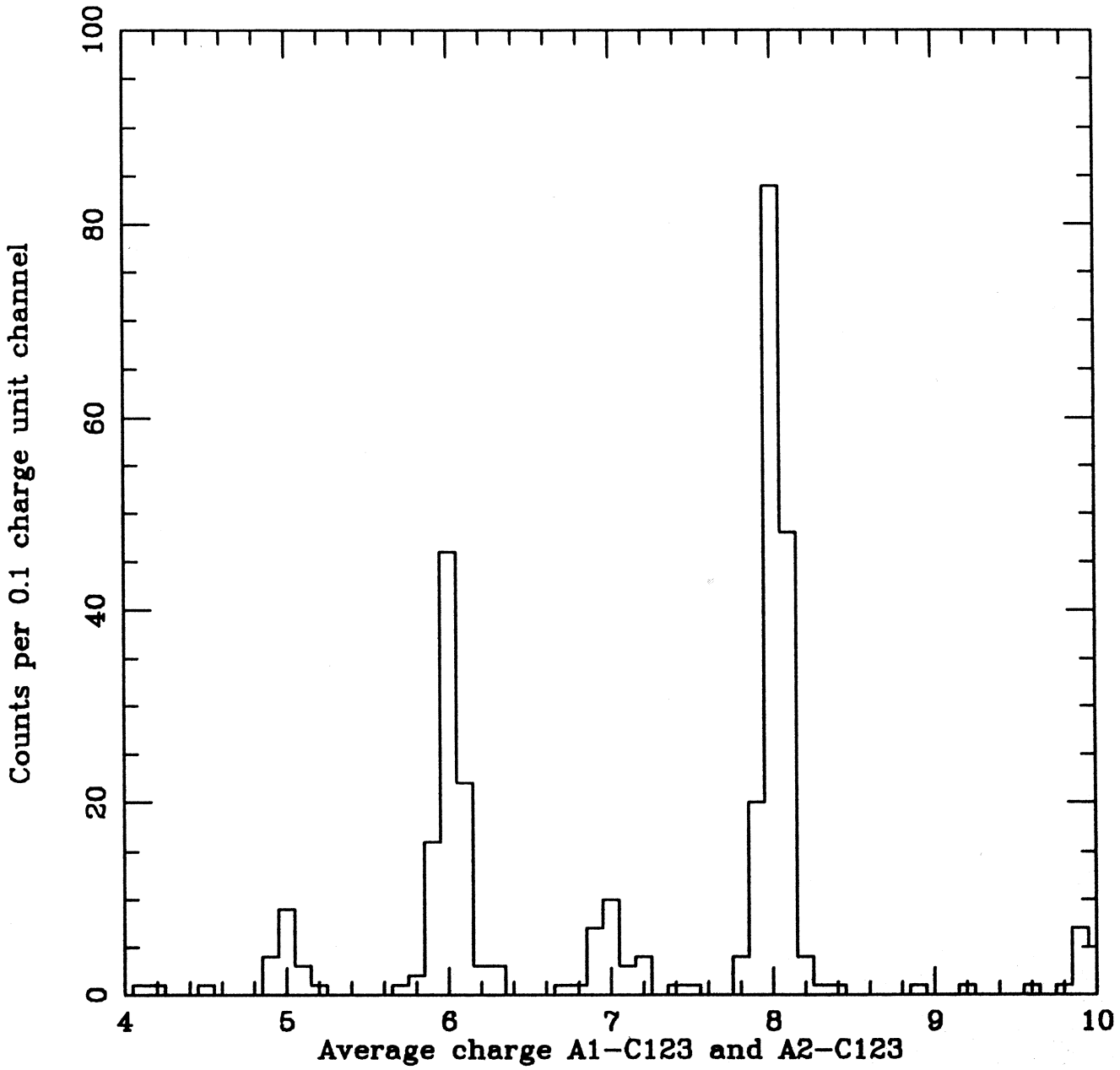

data file: s4v177ast.dat

 # evts read: 478

422evts selected with |Z2-Z1| < 3.00 sigma

sigma = 0.0550 + 0.0055*zav

Voyager-1, HET-II

12/1/77 - 4/1/78

Low Gain

A-stopping events

Fig.19 Number of counts versus charge Z for A-stopping events registered by Voyager-1 detector HET-II in the time period of 12/1/77 to 4/1/78.

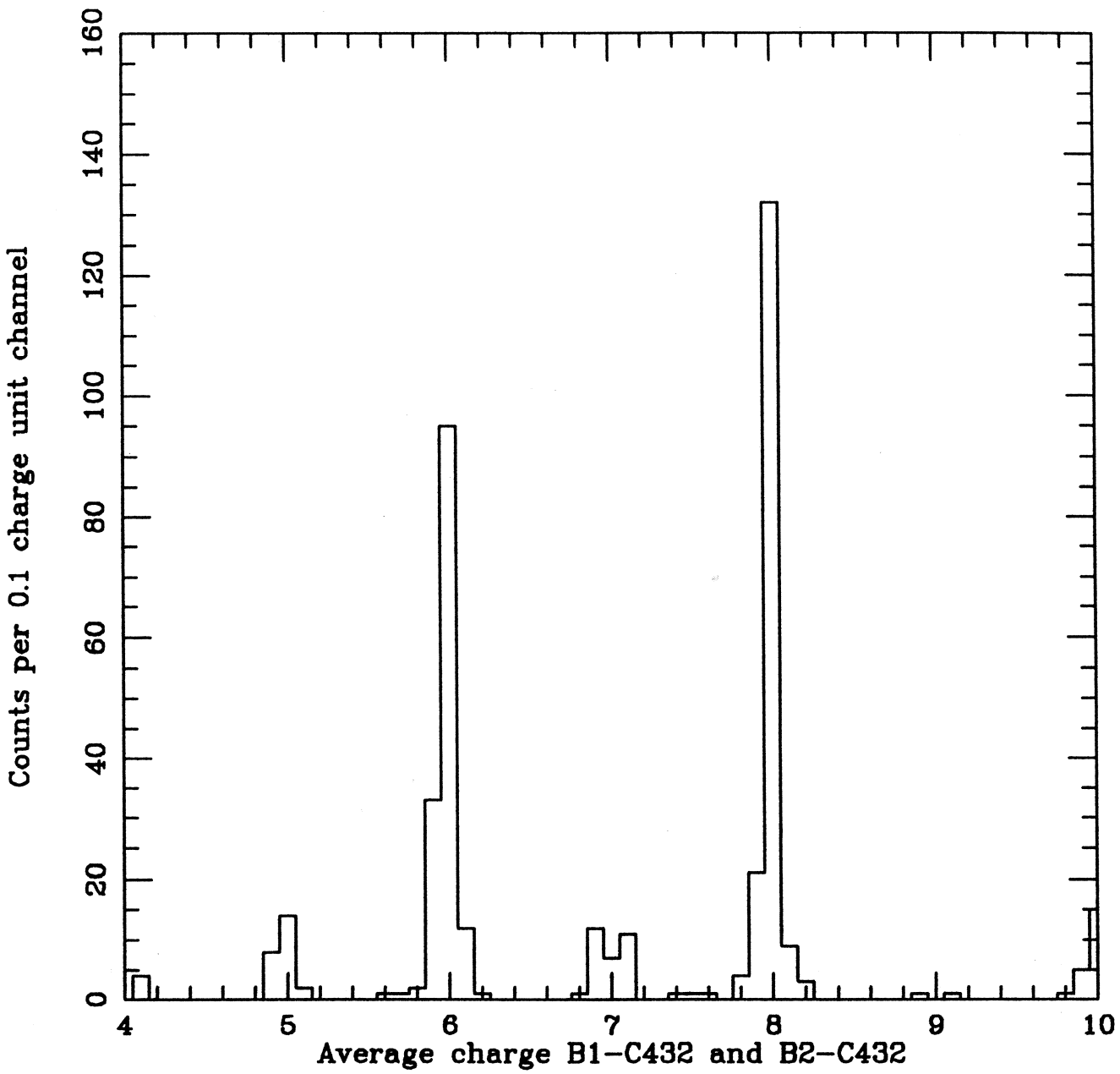

data file: s4v177bst.dat

 # evts read: 749

622evts selected with |Z2-Z1| < 3.00 sigma

sigma = 0.0550 + 0.0055*zav

Voyager-1, HET-II

12/1/77 - 4/1/78

Low Gain

B-stopping events

Fig.20 Number of counts versus charge Z for B-stopping events registered by Voyager-1 detector HET-II in the time period of 12/1/77 to 4/1/78.

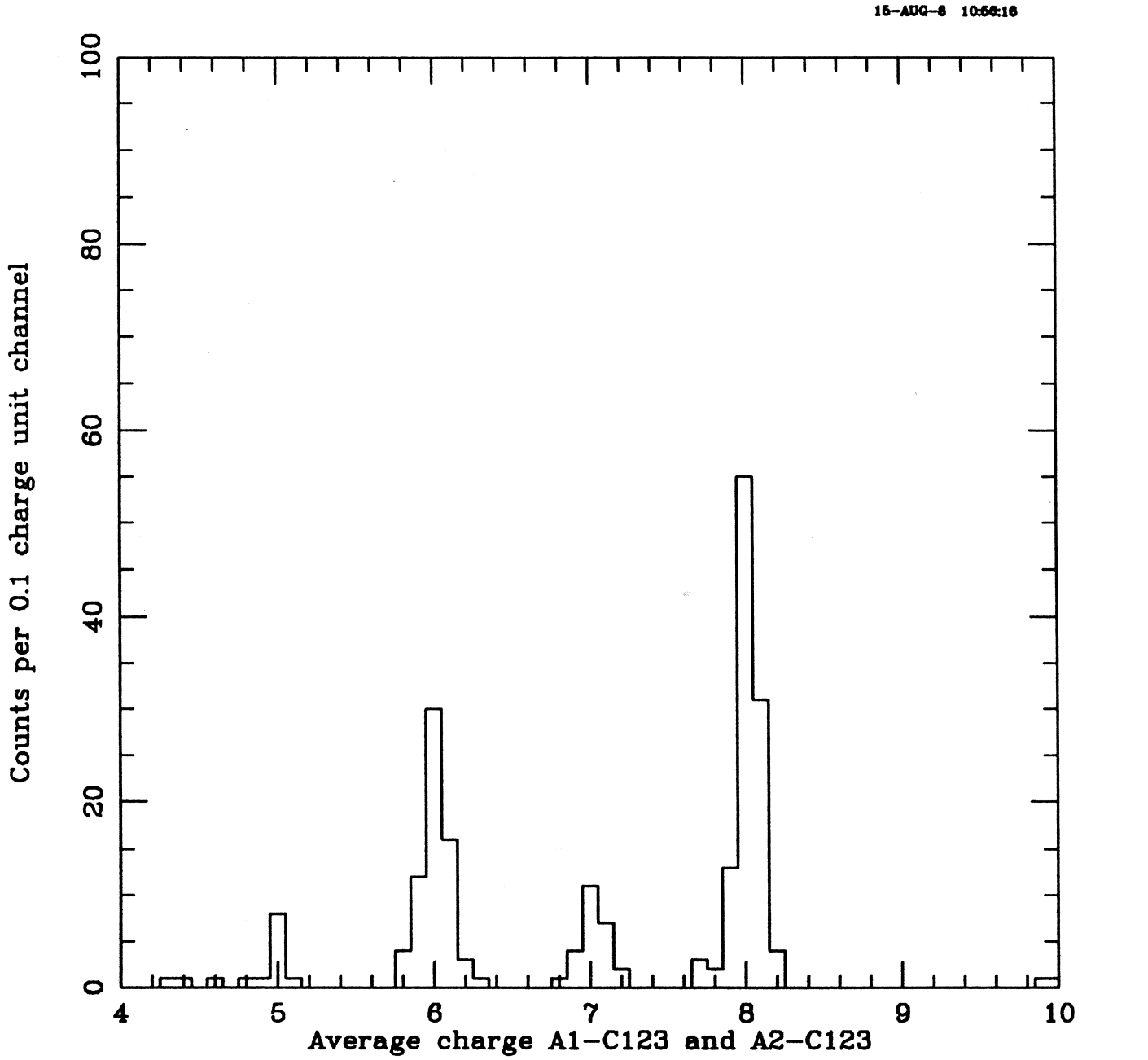

Fig.21 Number of counts versus charge Z for A-stopping events registered by Voyager-2 detector HET-I in the time period of 12/1/77 to 4/1/78.

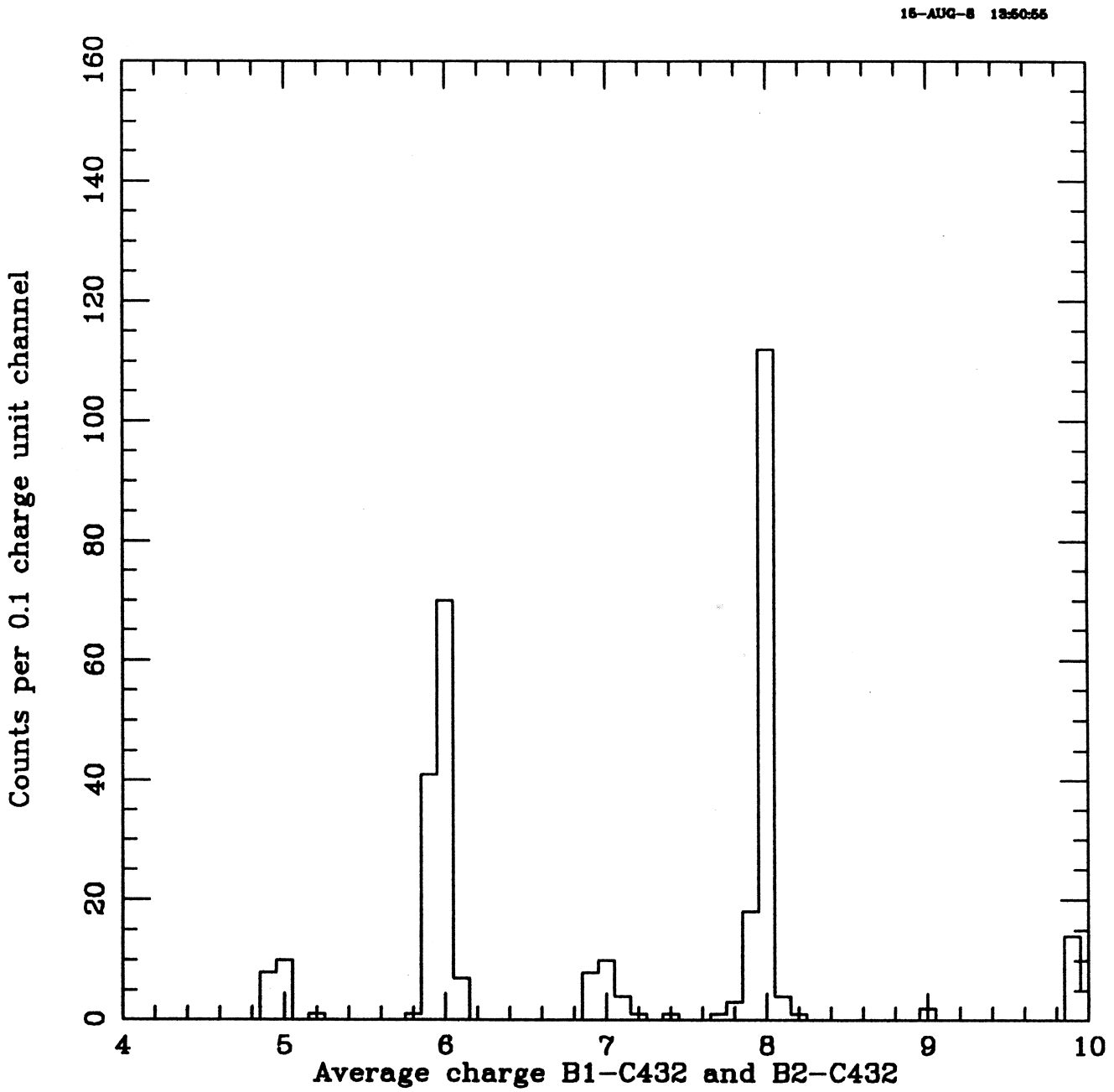

Fig.22 Number of counts versus charge Z for B-stopping events registered by Voyager-2 detector HET-I in the time period of 12/1/77 to 4/1/78.

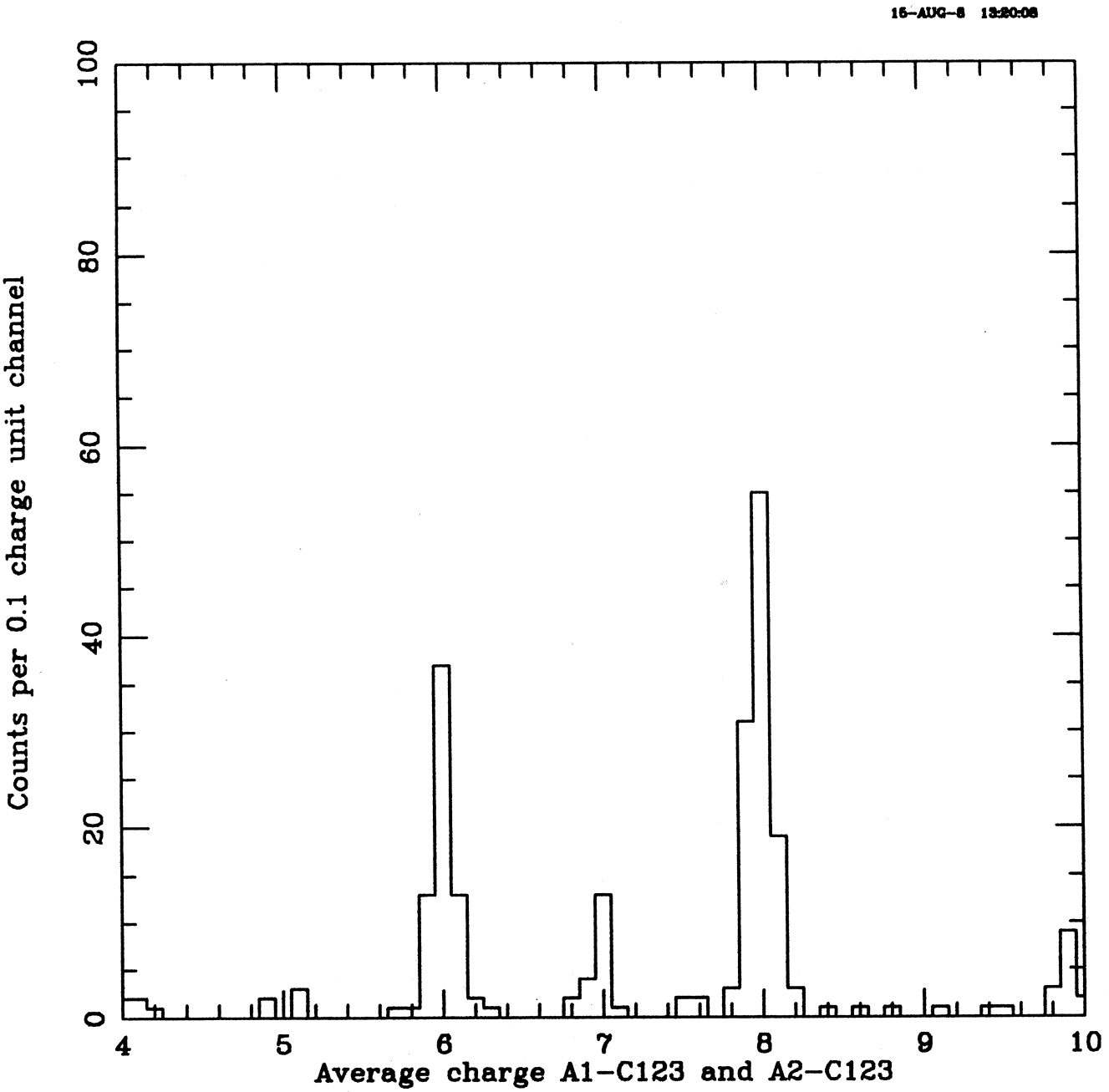

Fig.23 Number of counts versus charge Z for A-stopping events registered by Voyager-2 detector HET-II in the time period of 12/1/77 to 4/1/78.

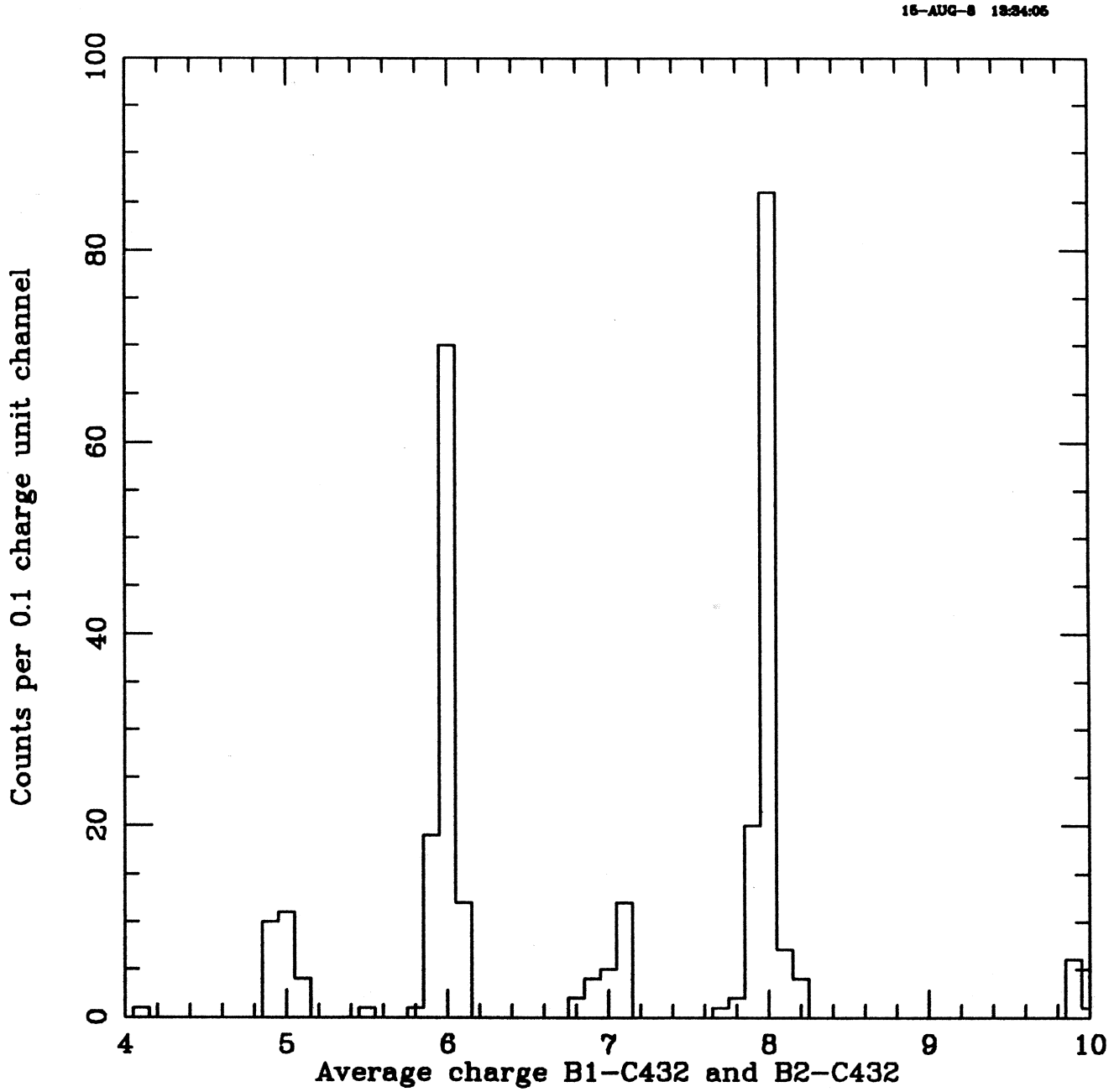

data file: s4v22b7_8.dat

 # evts read: 475

397evts selected with |Z2-Z1| < 3.00 sigma

sigma = 0.0550 + 0.0055*zav

Voyager-2, HET-II
12/1/77 - 4/1/78
Low Gain
B-stopping events

Fig.24 Number of counts versus charge Z for B-stopping events registered by Voyager-2 detector HET-II in the time period of 12/1/77 to 4/1/78.

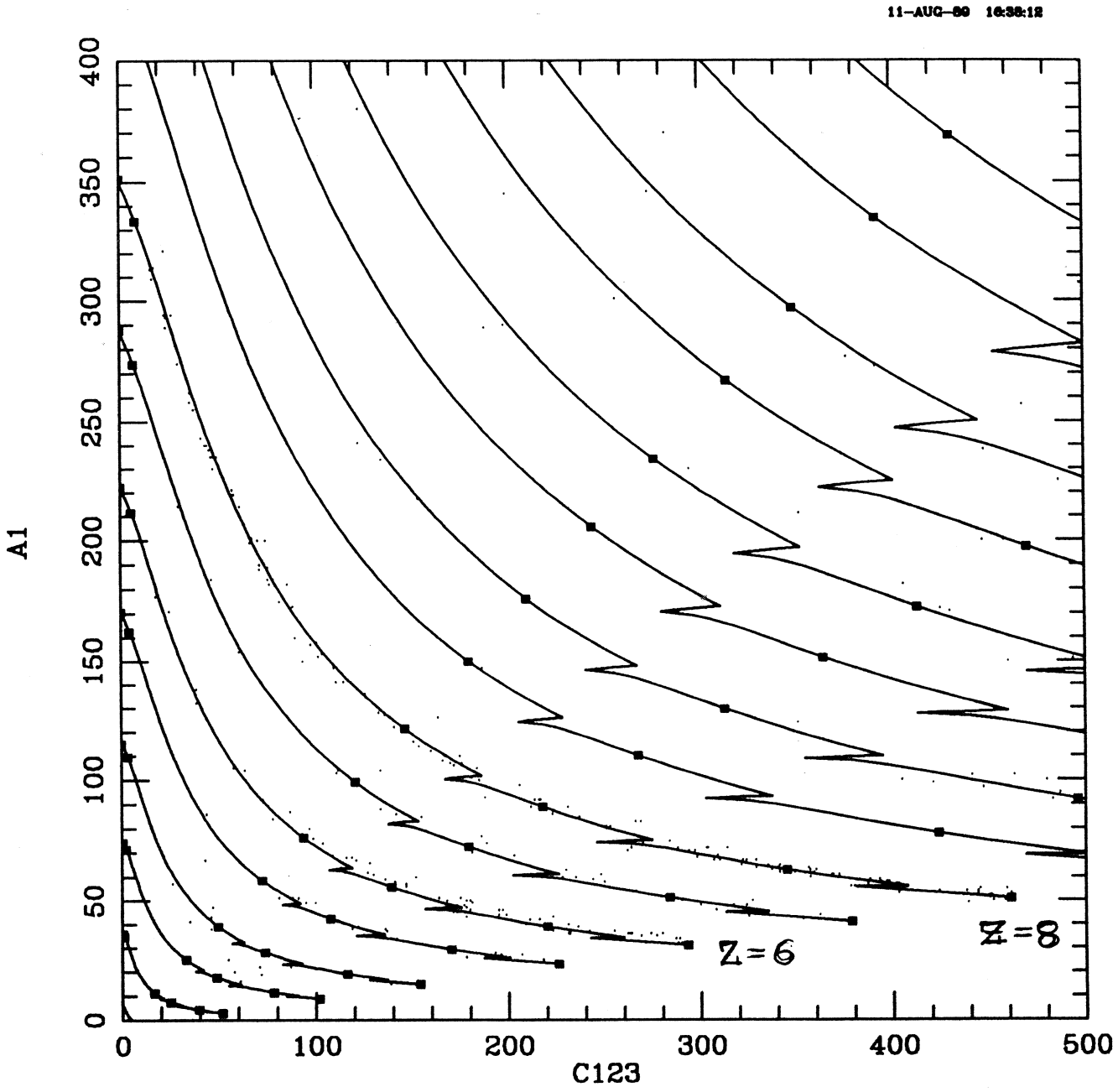

data file: s3v11a7_8.dat

evts read and selected: 490 444

|z2−z1| < 3.00*sigma, with sigma = 0.0550 + 0.0055*z

Energy bins from: ebv11a.dat

simulation file: trv1h1.sim

Offset D1, D2, C: −3.00 −3.00 0.00

FSMeV D1, D2, C: 850. 850. 17300.

Voyager-1

HET-I

12/1/77 - 4/1/78

Low Gain events

Fig.25 Fit of simulation tracks to A-stopping experimental events (Voyager-1, HET-I) registered in the time period of 12/1/77 to 4/1/78. The events are represented by energies deposited in A1 and C123 detector layers.

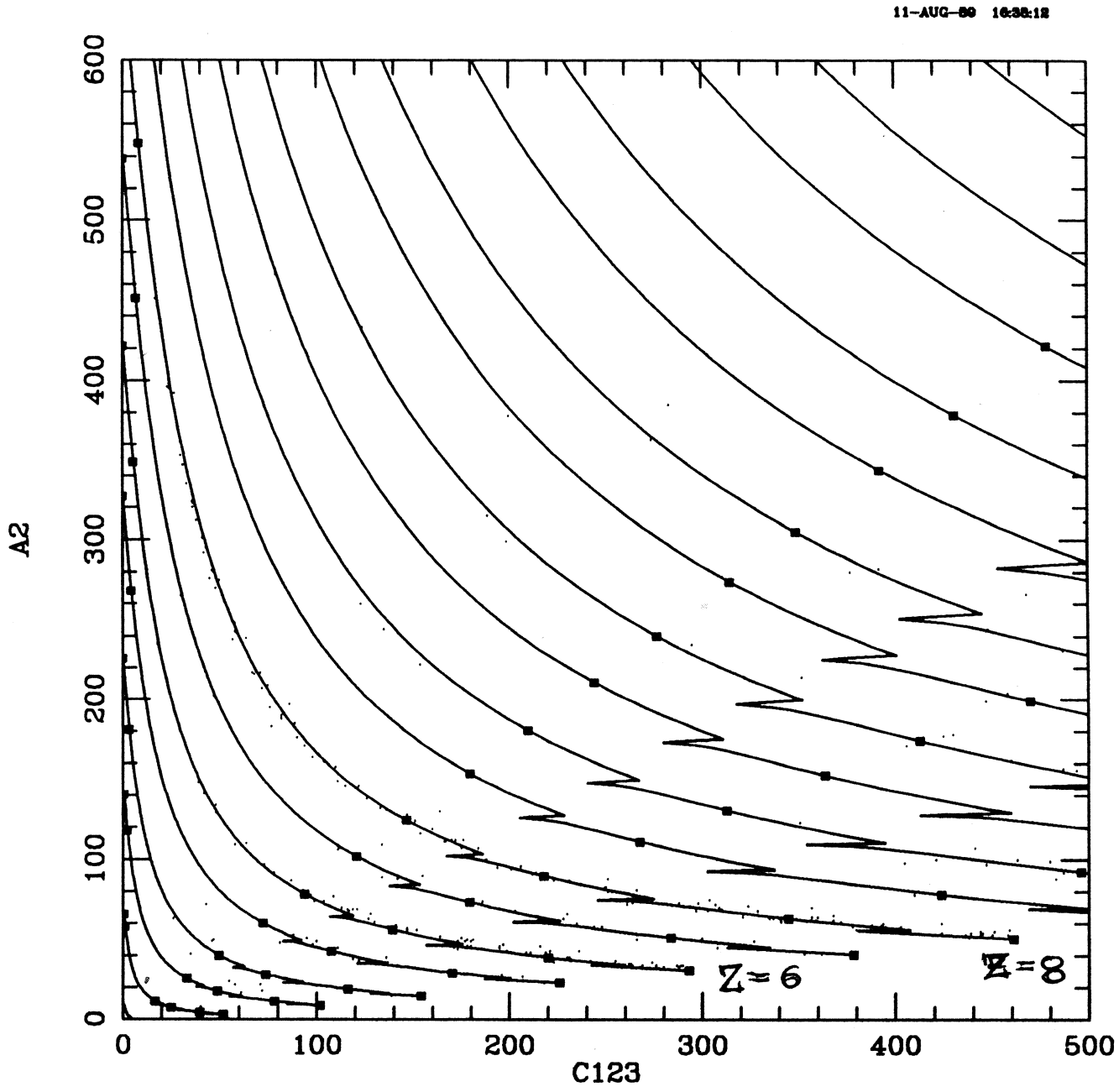

data file: s3v11a7_8.dat

evts read and selected: 490 444

|z2−z1| < 3.00*sigma, with sigma = 0.0550 + 0.0055*z

Energy bins from: ebv11a.dat

simulation file: trv1h1.sim

Offset D1, D2, C: −3.00 −3.00 0.00

FSMeV D1, D2, C: 850. 850. 17300.

Voyager - 1

HET - I

12/1/77 - 4/1/78

Low Gain events

Fig.26 The same as in Fig.25 for the energies deposited in A2 and C123 detector layers.

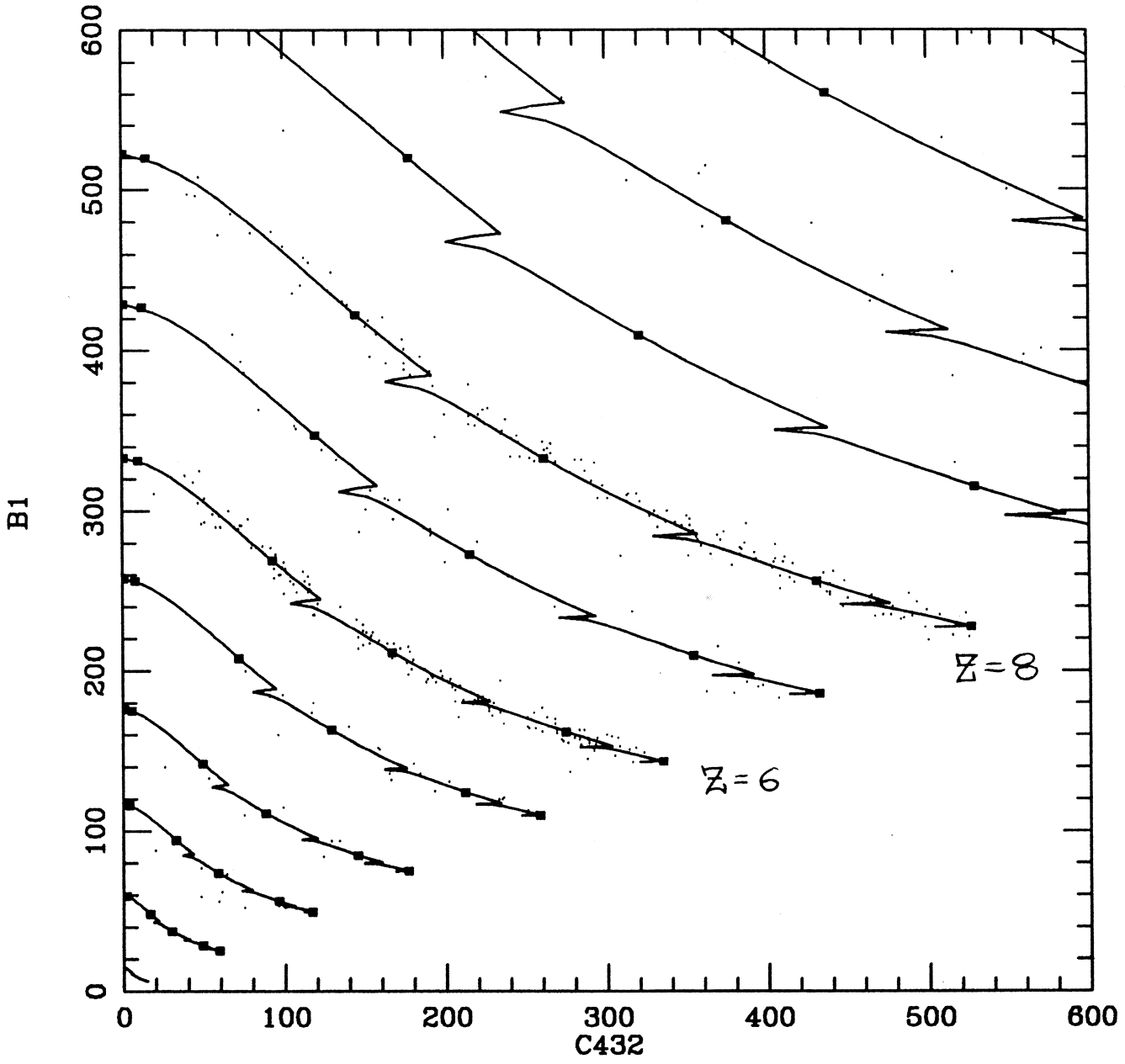

data file: s3v11b7_8.dat

evts read and selected: 655 553

|z2−z1| < 3.00*sigma, with sigma = 0.0550 + 0.0055*z

Energy bins from: ebv11b.dat

simulation file: trv1h1.sim

Offset D1, D2, C: 0.00 0.00 0.00

FSMeV D1, D2, C: 2300. 4180. 16850.

Voyager-1
HET-I
12/1/77-4/1/78
Low Gain Events

Fig.27 The same as in Fig.25 for the energies deposited in B1 and C432 detector layers.

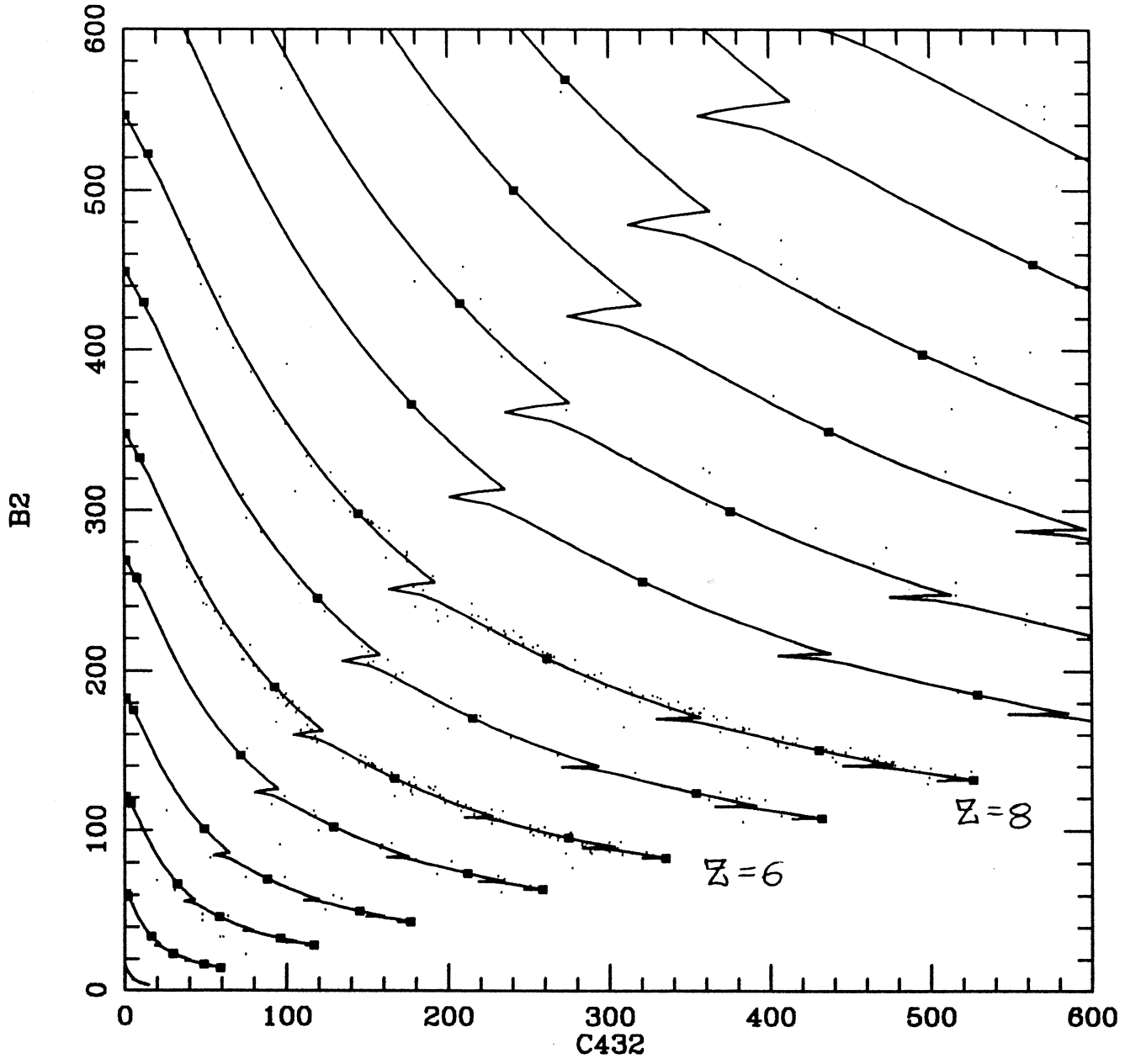

data file: s3v11b7_8.dat

evts read and selected: 655 553

|z2−z1| < 3.00*sigma, with sigma = 0.0550 + 0.0055*z

Energy bins from: ebv11b.dat

simulation file: trv1h1.sim

Offset D1, D2, C: 0.00 0.00 0.00

FSMeV D1, D2, C: 2300. 4180. 16850.

Voyager-1
HET-I
12/1/77-4/1/78
Low Gain Events

Fig.28 The same as in Fig.25 for the energies deposited in B2 and C432 detector layers.

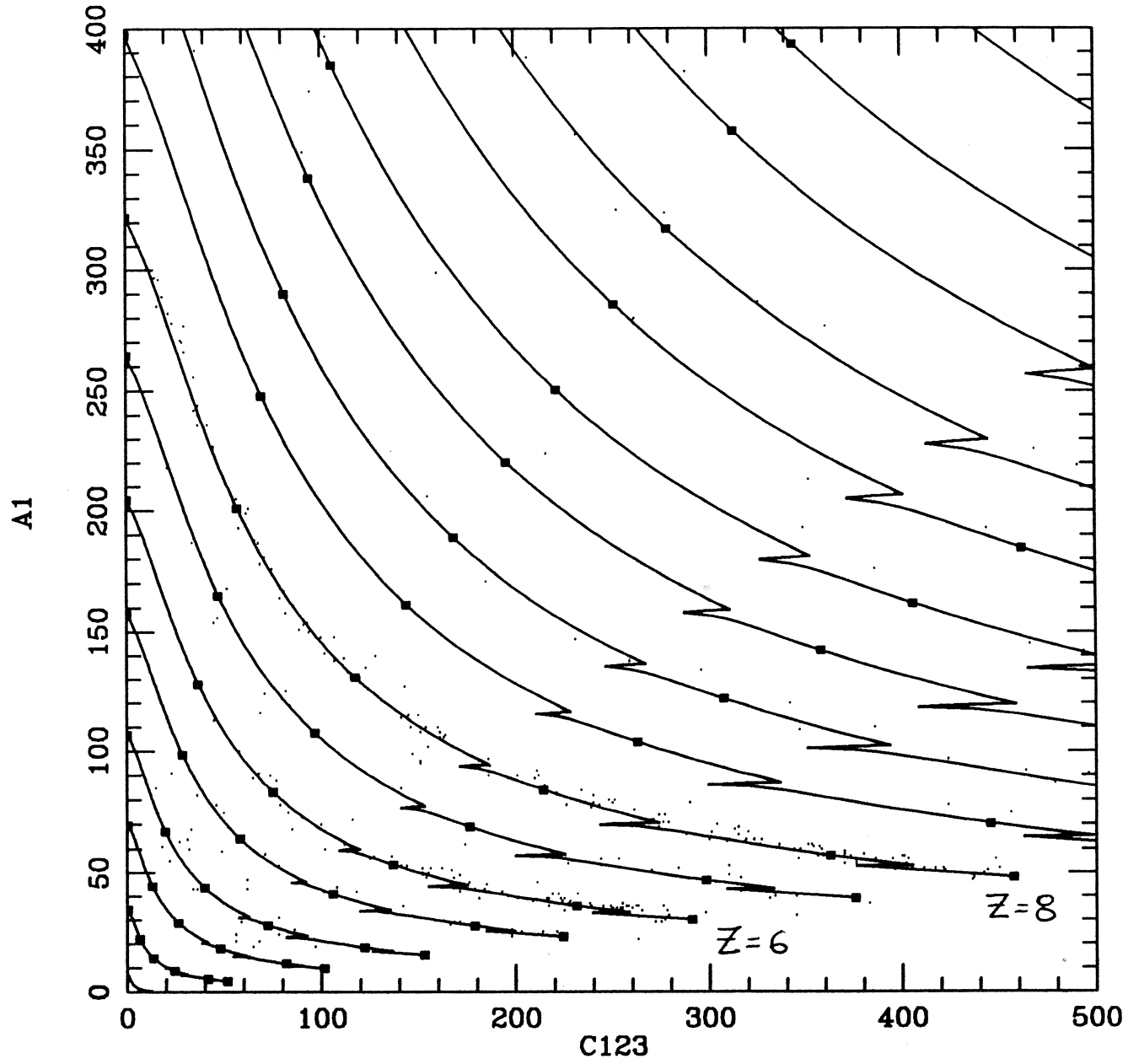

Voyager - 1, HET-II

12/1/77 - 4/1/78

data file: s4v177ast.dat

# evts read and selected:	478	478

No selection on charge consistency

Energy bins from: binsv1as.dat

simulation file: repv1dl1.sim

Offset D1, D2, C:	−1.00	0.00	0.00
FSMeV D1, D2, C:	935.	915.	17400.

Fig.29 Fit of simulation tracks to A-stopping experimental events (Voyager-1, HET-II) registered in the time period of 12/1/77 to 4/1/78. The events are represented by energies deposited in A1 and C123 detector layers.

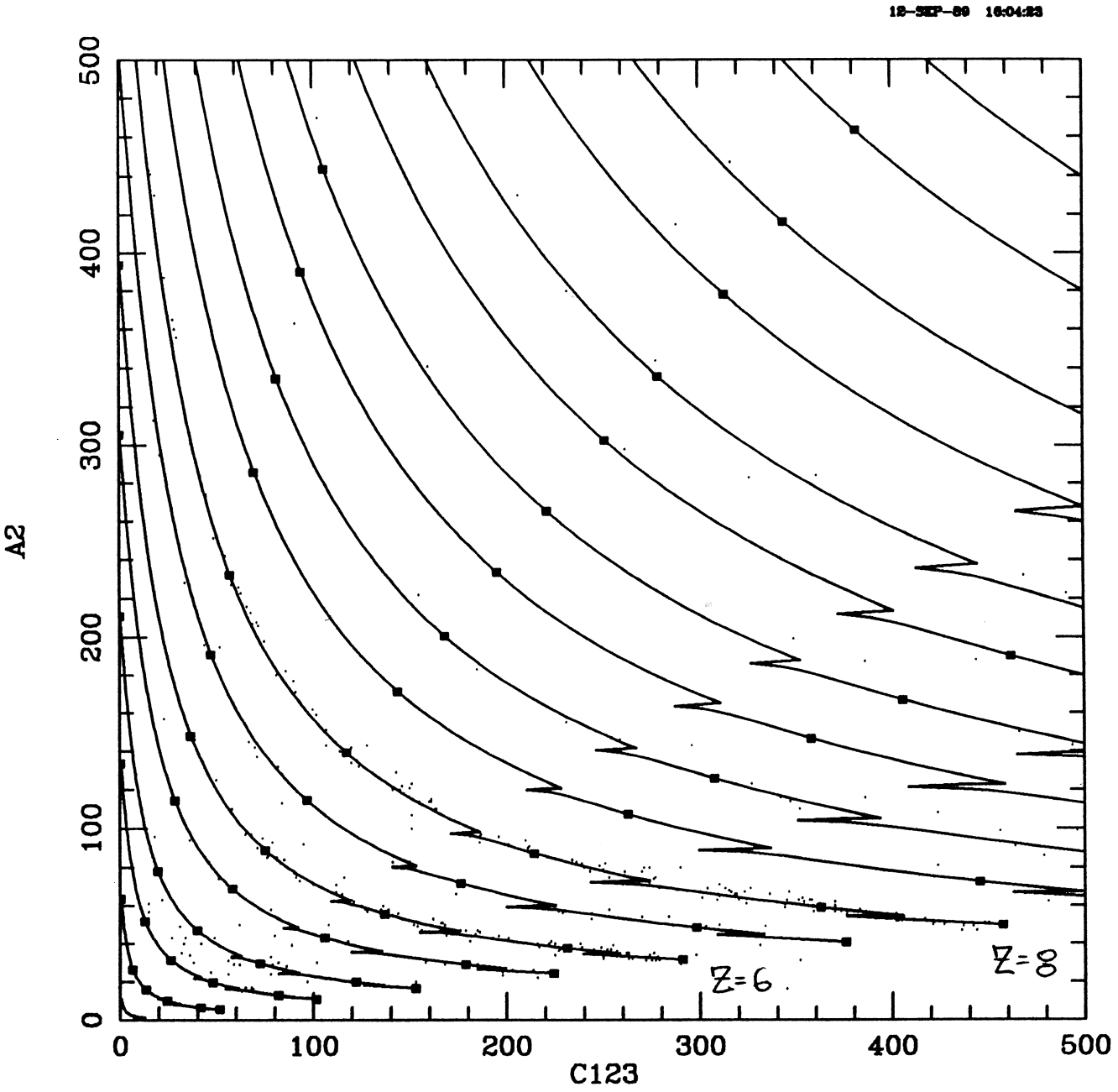

data file: s4v177ast.dat

evts read and selected: 478 478

No selection on charge consistency

Energy bins from: binsv1as.dat

simulation file: repv1dl1.sim

Offset D1, D2, C: −1.00 0.00 0.00

FSMeV D1, D2, C: 935. 915. 17400.

Voyager-1, HET-I

12/1/77 − 4/1/78

Fig.30 The same as in Fig.29 for the energies deposited in A2 and C123 detector layers.

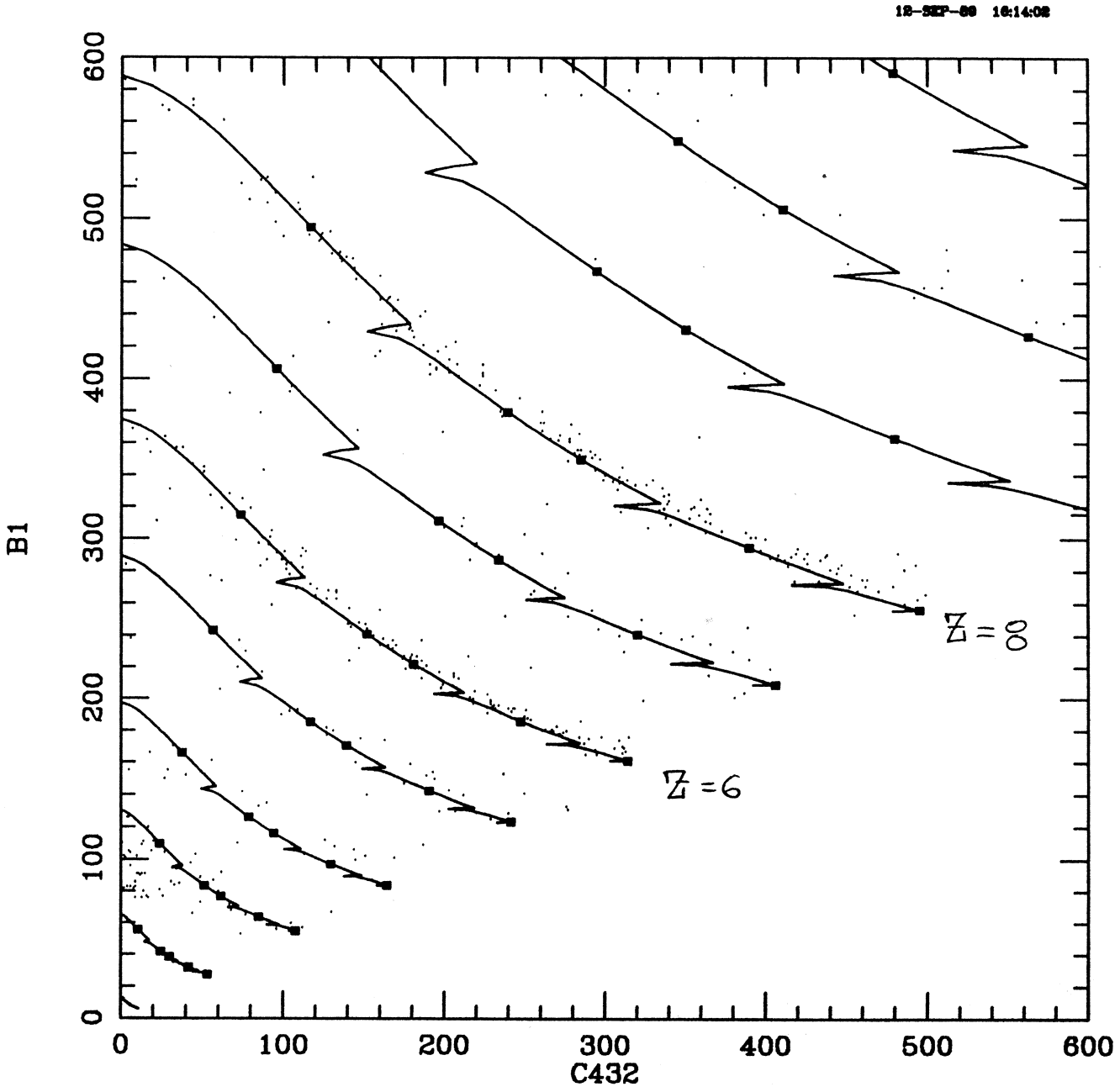

data file: s4v177bst.dat

# evts read and selected:	749	749
No selection on charge consistency		
Energy bins from: binsv1bs.dat		
simulation file: repv1dl1.sim		
Offset D1, D2, C:	−1.00	0.00 −3.00
FSMeV D1, D2, C:	2060.	4170. 17750.

Voyager-1, HET-II
12/1/77 - 4/1/78

Fig.31 The same as in Fig.29 for the energies deposited in B1 and C432 detector layers.

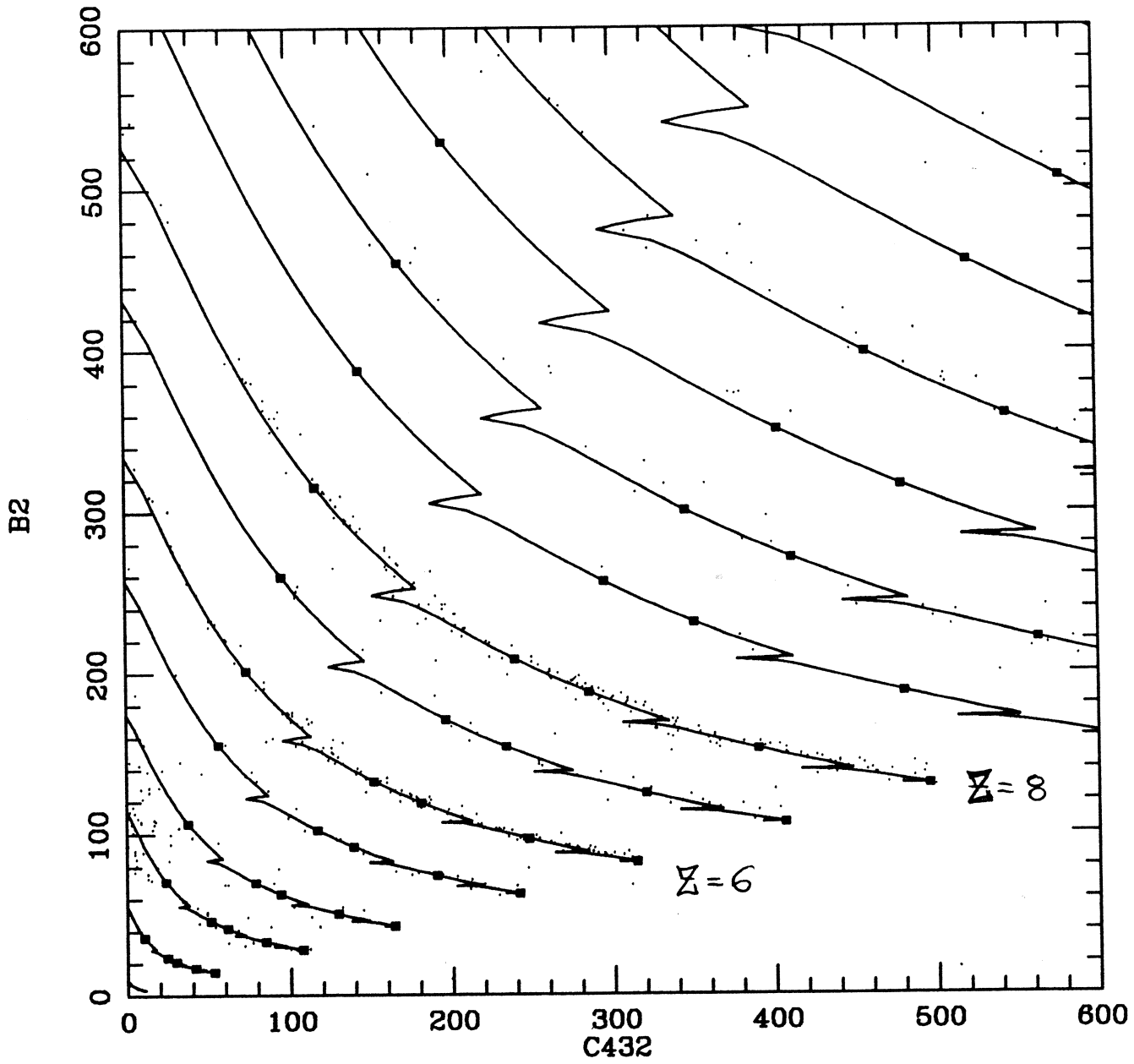

data file: s4v177bst.dat

Voyager-1, HET-II

# evts read and selected:	749	749	12/1/77 -4/1/78
No selection on charge consistency			
Energy bins from: binsv1bs.dat			
simulation file: repv1dl1.sim			
Offset D1, D2, C:	−1.00	0.00	−3.00
FSMeV D1, D2, C:	2060.	4170.	17750.

Fig.32 The same as in Fig.29 for the energies deposited in B2 and C432 detector layers.

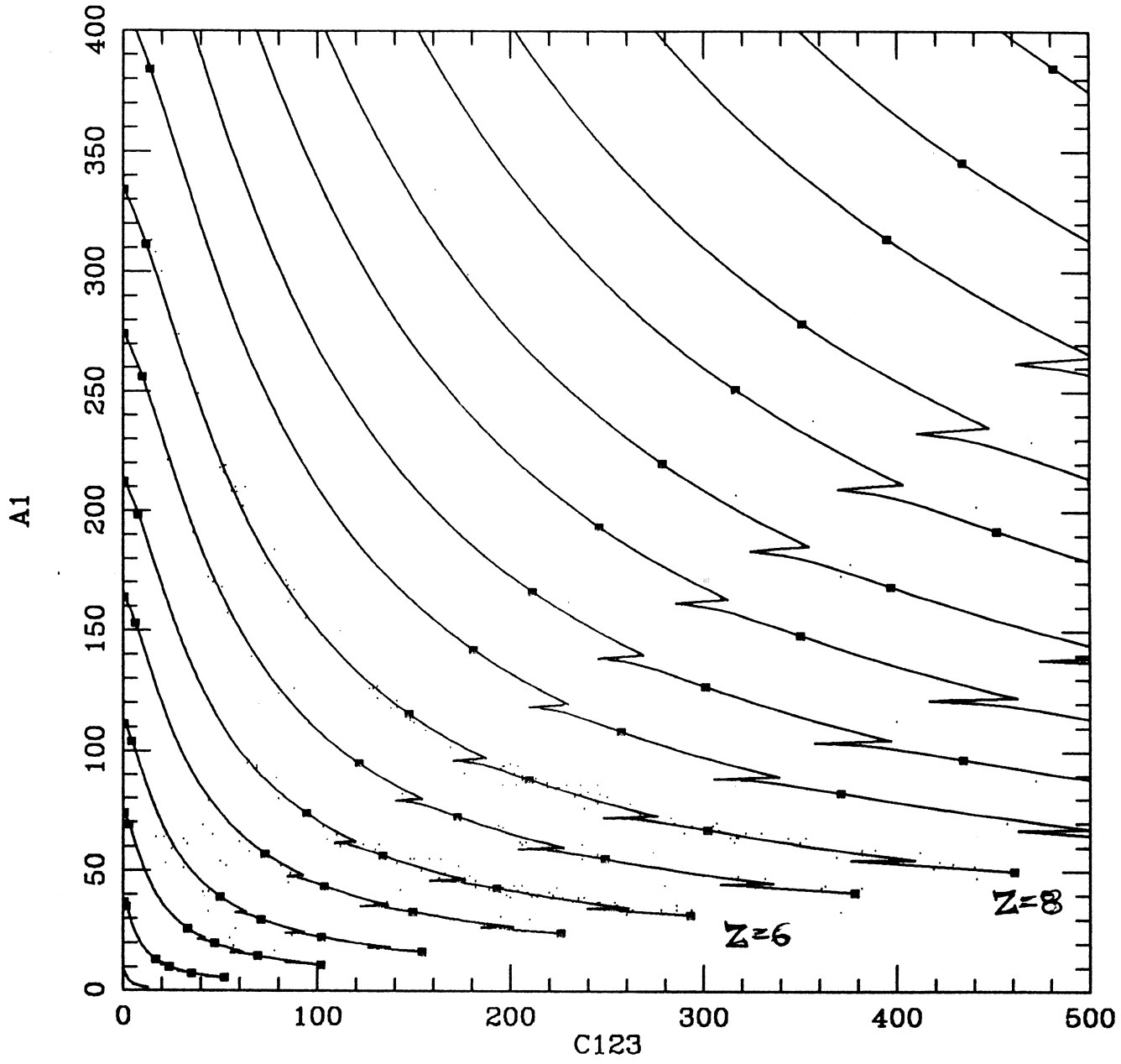

data file: s4v21a7_8.dat

evts read and selected: 330 330

No selection on charge consistency

Energy bins from: ebz6v21a.dat

simulation file: trv2h1.sim

Offset D1, D2, C: 0.00 2.00 0.00

FSMeV D1, D2, C: 890. 925. 17250.

Voyager-2, HET-I

Time Period:

12/1/77 - 4/1/78

Low Gain events

Fig.33 Fit of simulation tracks to A-stopping experimental events (Voyager-2, HET-I) registered in the time period of 12/1/77 to 4/1/78. The events are represented by energies deposited in A1 and C123 detector layers.

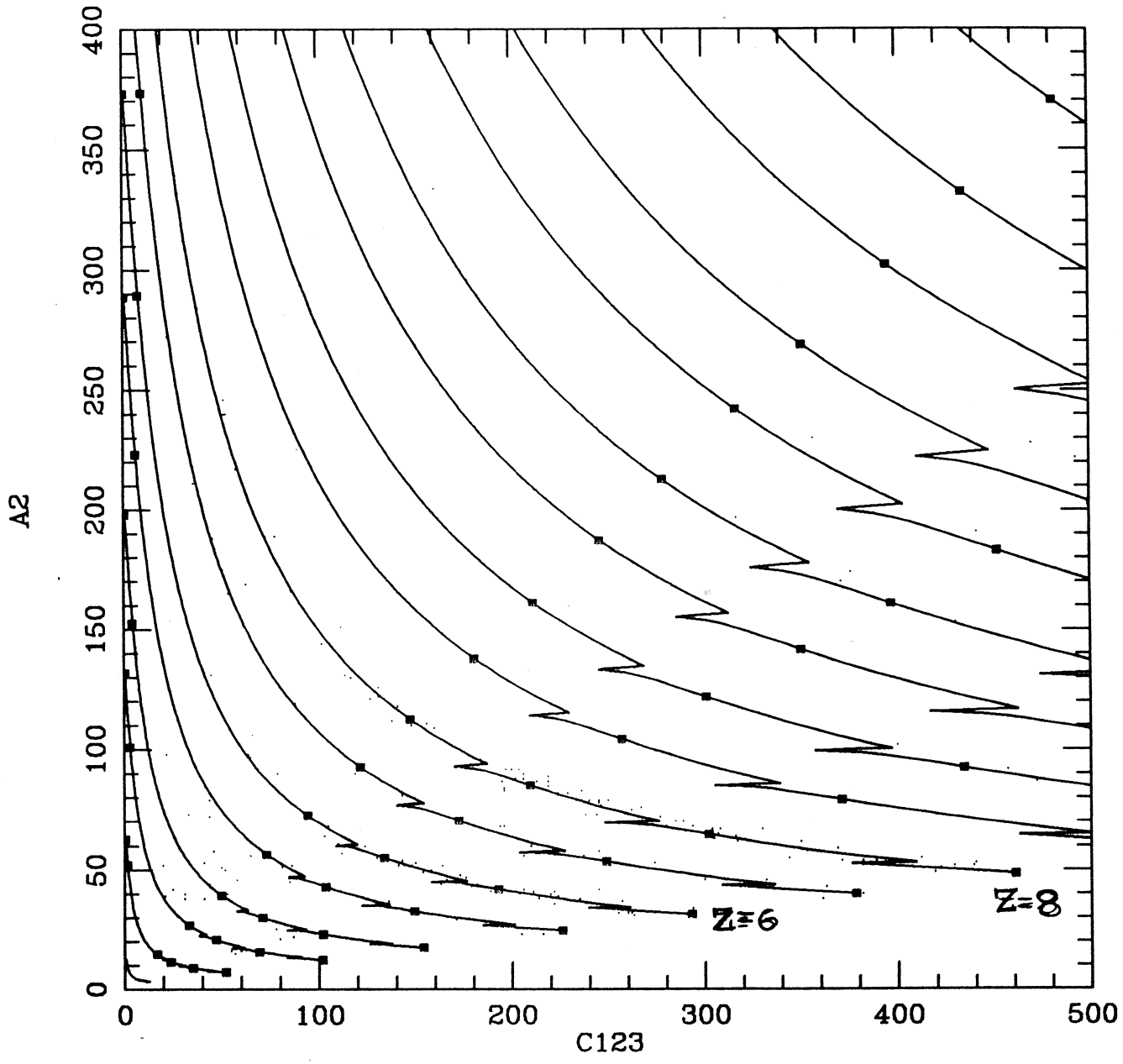

data file: s4v21a7_8.dat

# evts read and selected:	330	330

No selection on charge consistency

Energy bins from: ebz6v21a.dat

simulation file: trv2h1.sim

Offset D1, D2, C:	0.00	2.00	0.00
FSMeV D1, D2, C:	890.	925.	17250.

Voyager-2 HET-I

12/1/77 - 4/1/78

Low Gain events

Fig.34 The same as in Fig.33 for the energies deposited in A2 and C123 detector layers.

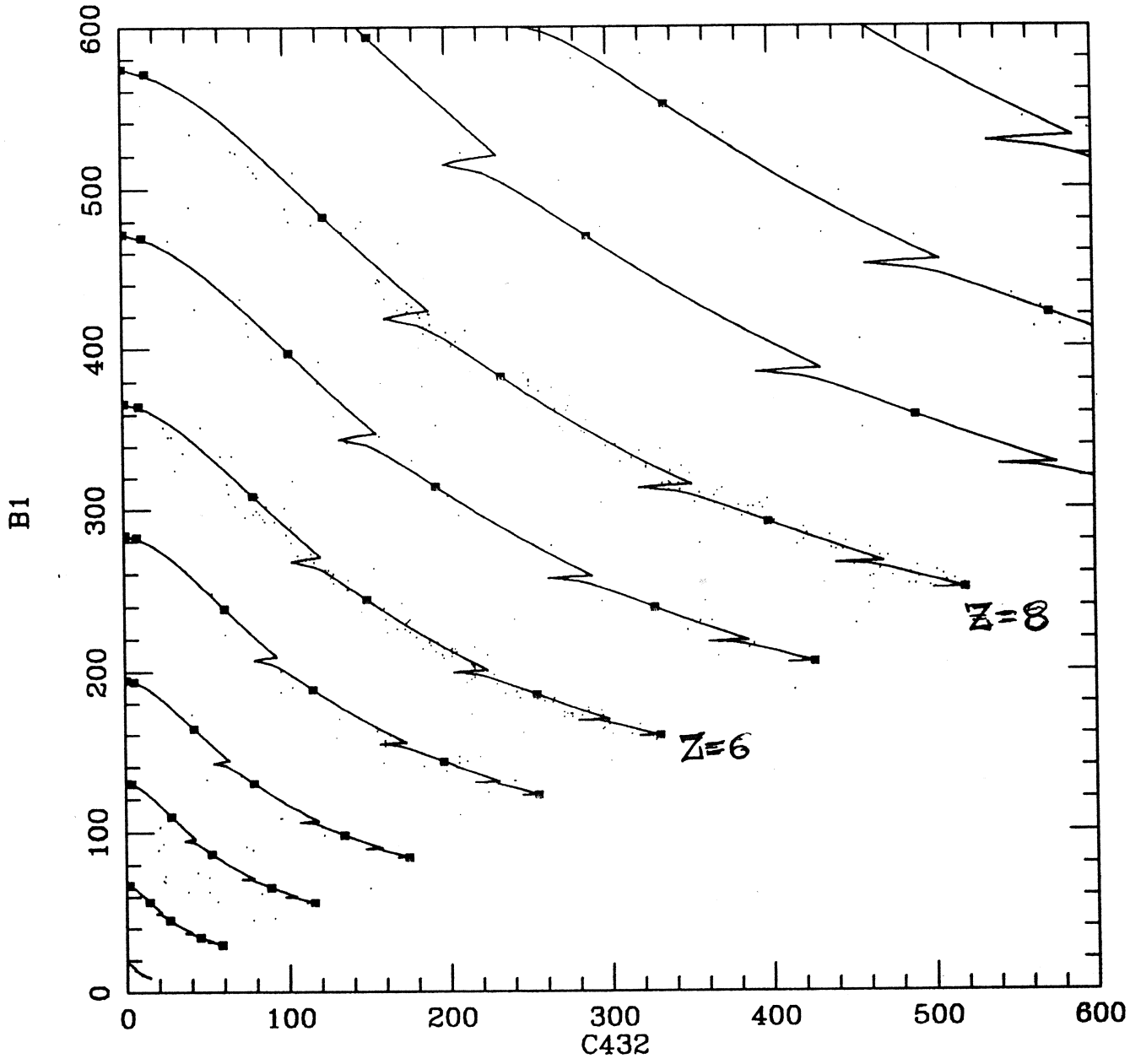

data file: s4v21b7_8.dat

# evts read and selected:	527	527

No selection on charge consistency

Energy bins from: ebz6v21b.dat

simulation file: trv2h1.sim

Offset D1, D2, C:	2.00	3.00	0.00
FSMeV D1, D2, C:	2100.	4120.	17050.

Voyager - 2, HET - I

Time period

12/1/77 - 4/1/78

Low Gain events

Fig.35 The same as in Fig.33 for the energies deposited in B1 and C432 detector layers.

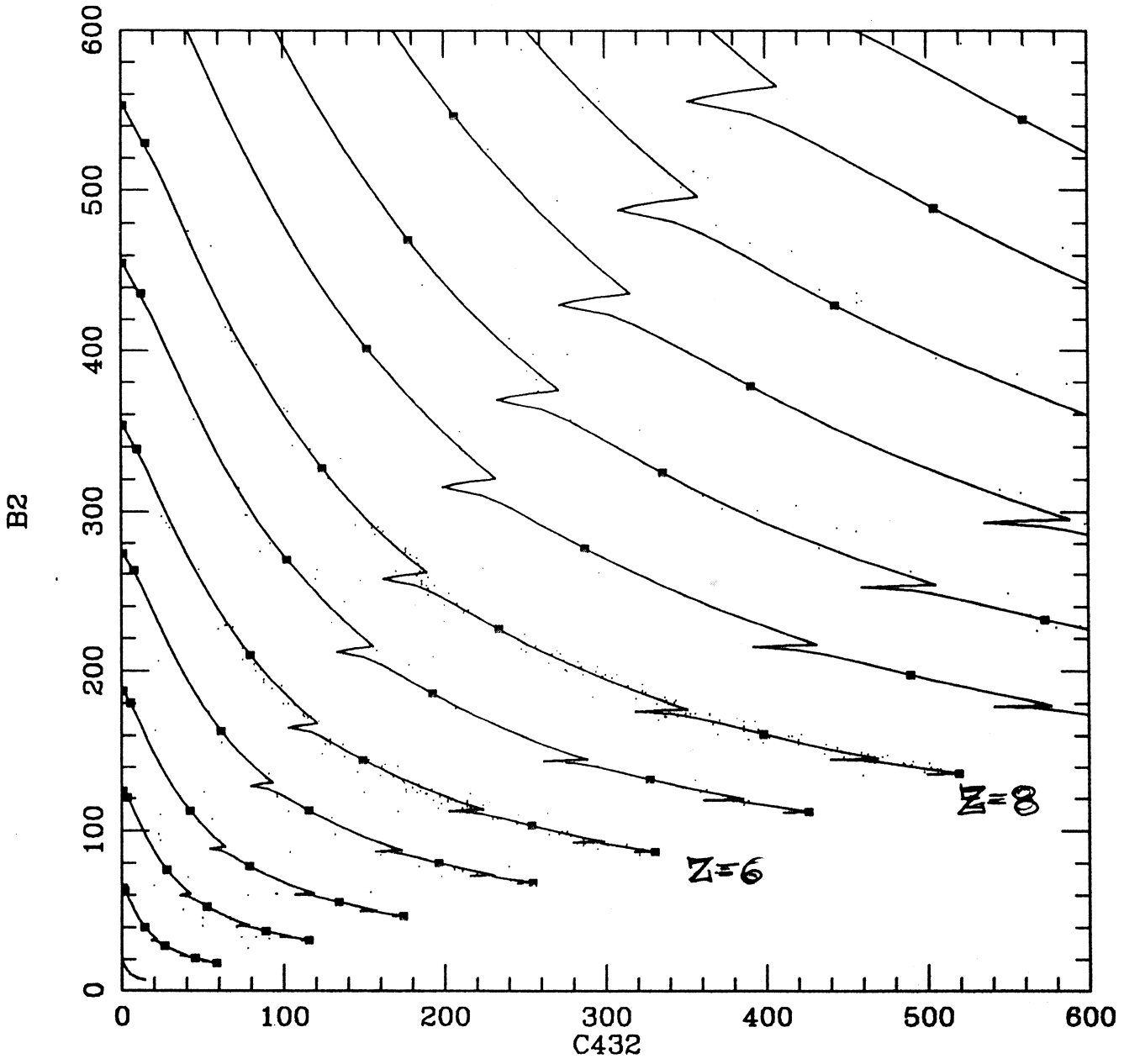

data file: s4v21b7_8.dat

# evts read and selected:	527	527

No selection on charge consistency

Energy bins from: ebz6v21b.dat

simulation file: trv2h1.sim

Offset D1, D2, C:	2.00	3.00	0.00
FSMeV D1, D2, C:	2100.	4120.	17050.

Voyager-2, HET-I

Time period

12/1/77 - 4/1/78

Low Gain events

Fig.36 The same as in Fig.33 for the energies deposited in B2 and C432 detector layers.

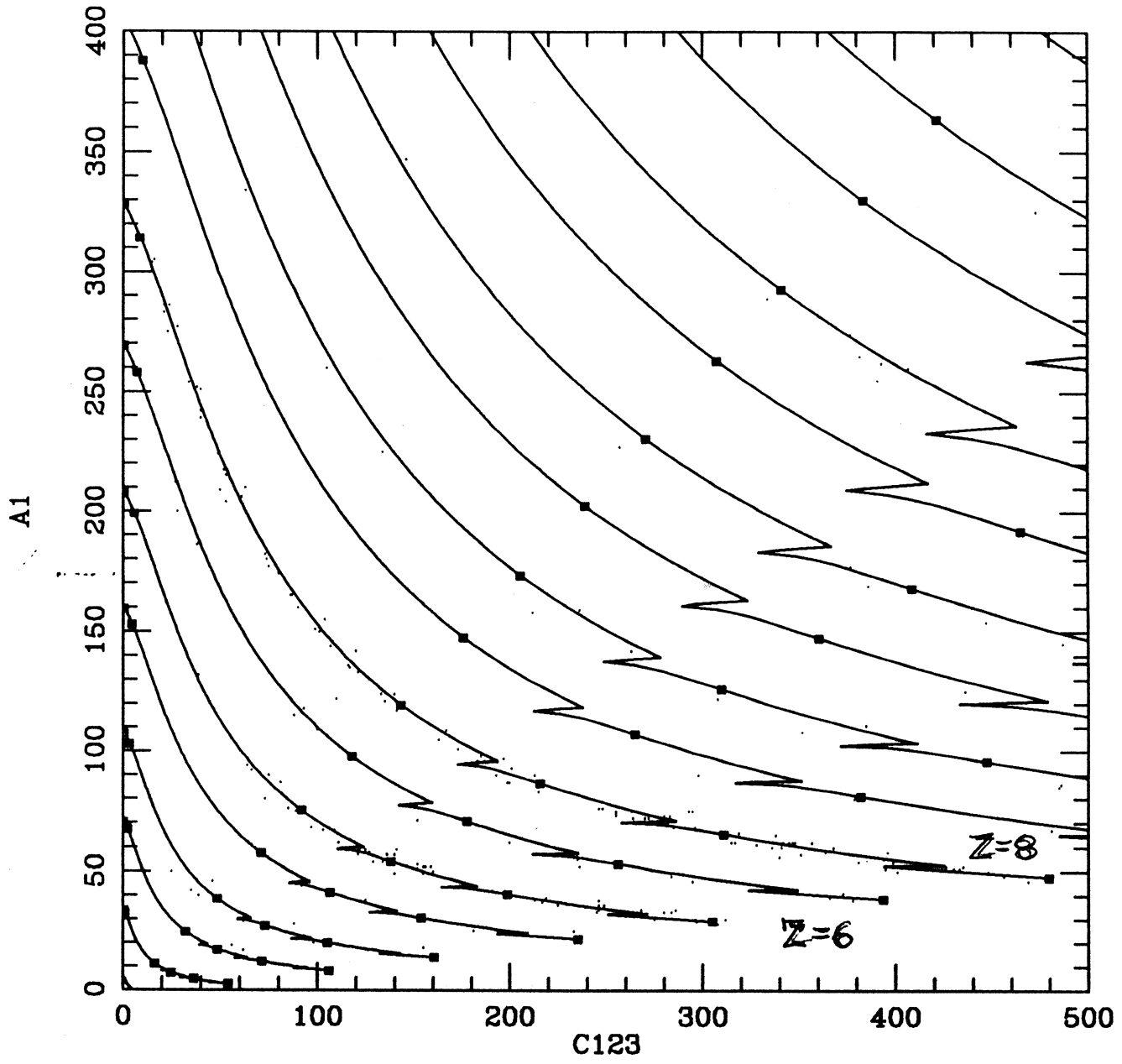

data file: s4v22a7_8.dat

evts read and selected: 368 323

|z2−z1| < 3.00*sigma, with sigma = 0.0550 + 0.0055*z

Energy bins from: ebinv22a.dat

simulation file: trv2h2.sim

Offset D1, D2, C:	−3.00	0.00	0.00
FSMeV D1, D2, C:	895.	860.	16600.

Voyager-2, HET-II

12/1/77 - 4/1/78

Low Gain events

Fig.37 Fit of simulation tracks to A-stopping experimental events (Voyager-2, HET-II) registered in the time period of 12/1/77 to 4/1/78. The events are represented by energies deposited in A1 and C123 detector layers.

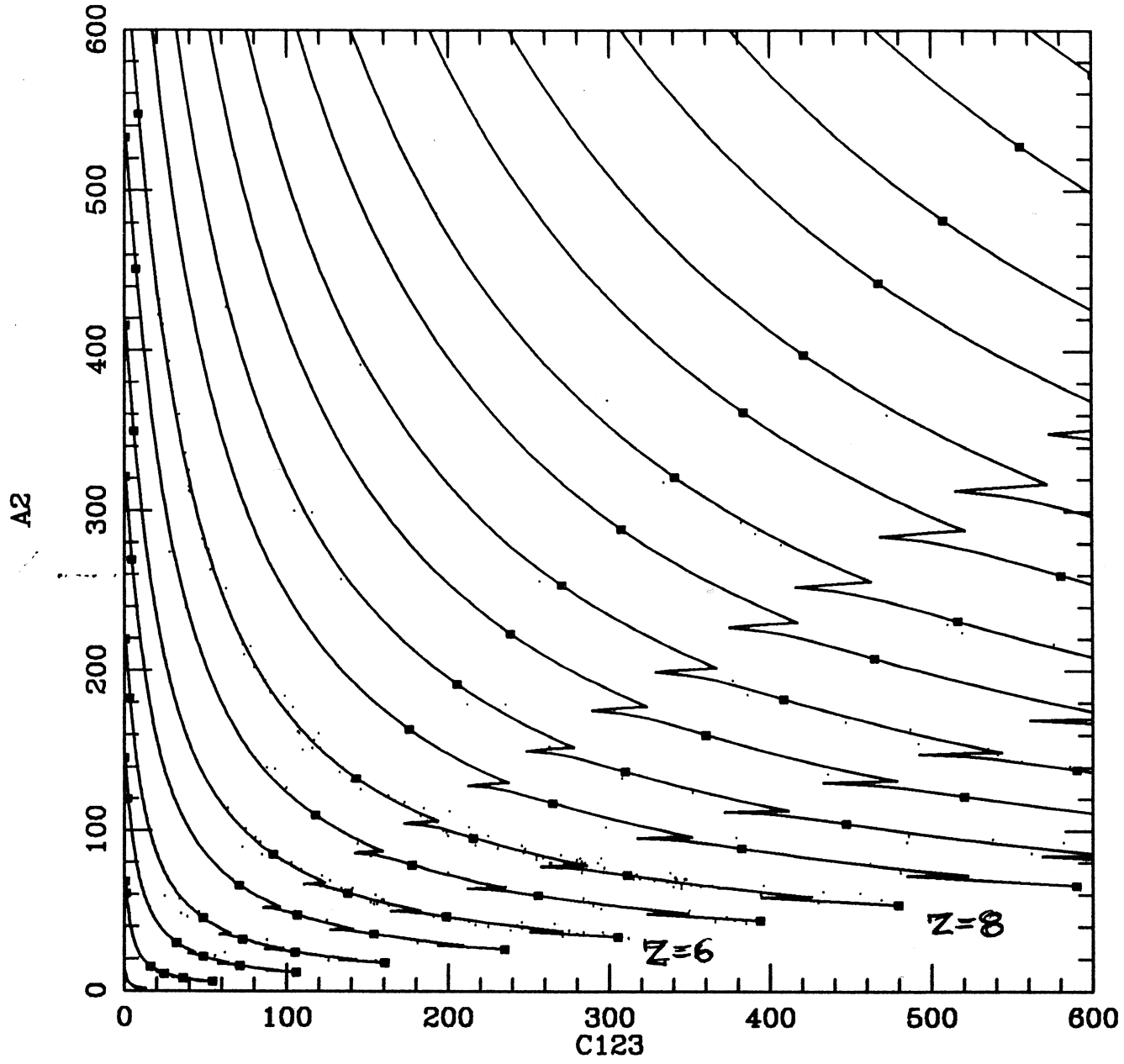

data file: s4v22a7_8.dat

evts read and selected: 368 323

|z2−z1| < 3.00*sigma, with sigma = 0.0550 + 0.0055*z

Energy bins from: ebinv22a.dat

simulation file: trv2h2.sim

Offset D1, D2, C: −3.00 0.00 0.00

FSMeV D1, D2, C: 895. 860. 16600.

Voyager - 2, HET-II

12/1/77 - 4/1/78

Low Gain events

Fig.38 The same as in Fig.37 for the energies deposited in A2 and C123 detector layers.

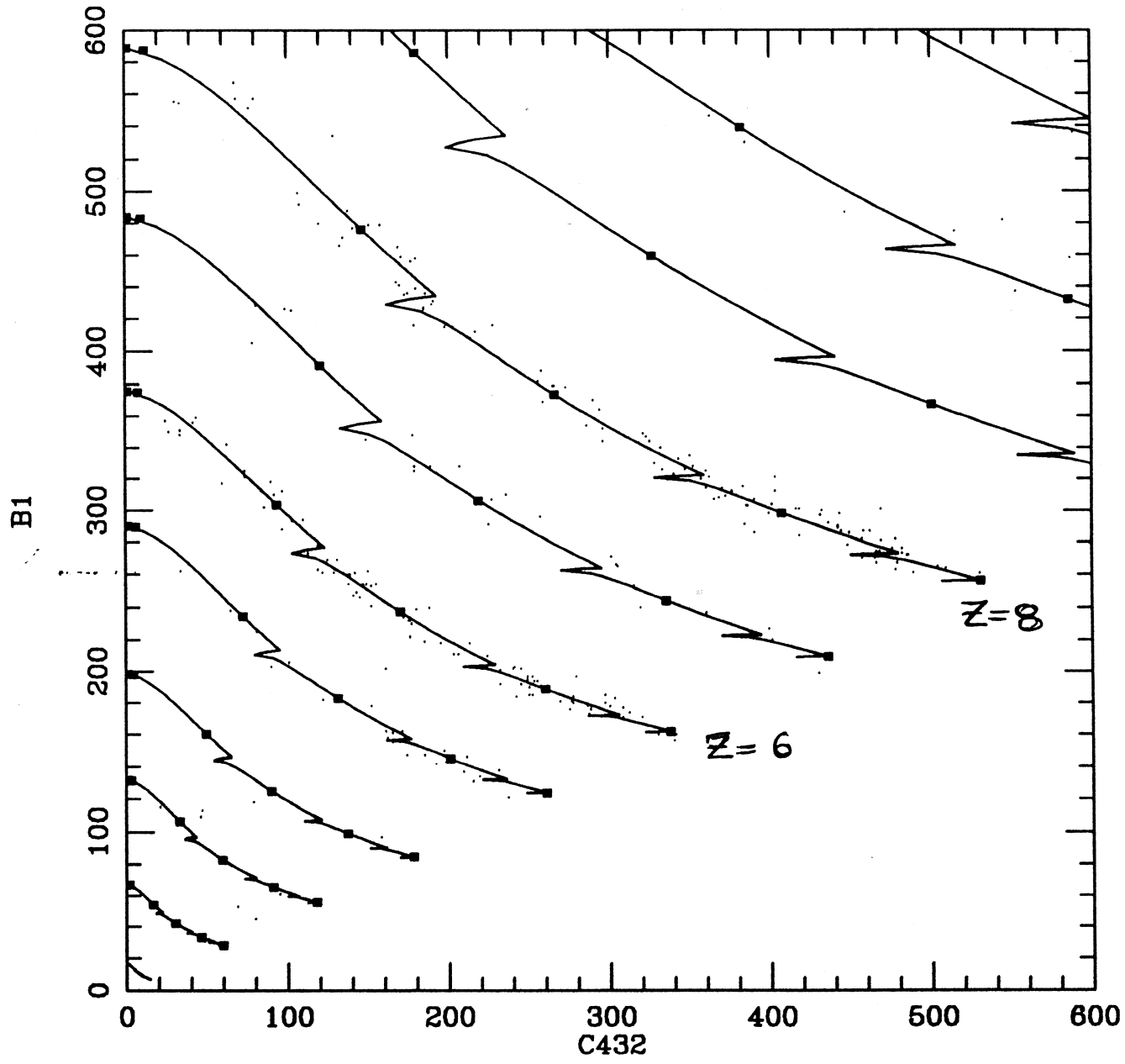

data file: s4v22b7_8.dat

evts read and selected: 475 397

|z2−z1| < 3.00*sigma, with sigma = 0.0550 + 0.0055*z

Energy bins from: ebinv22b.dat

simulation file: trv2h2.sim

Offset D1, D2, C:	0.00	0.00	0.00
FSMeV D1, D2, C:	2050.	4120.	16700.

Voyager-2, HET-II.
12/1/77 - 4/1/78
Low Gain events

Fig.39 The same as in Fig.37 for the energies deposited in B1 and C432 detector layers.

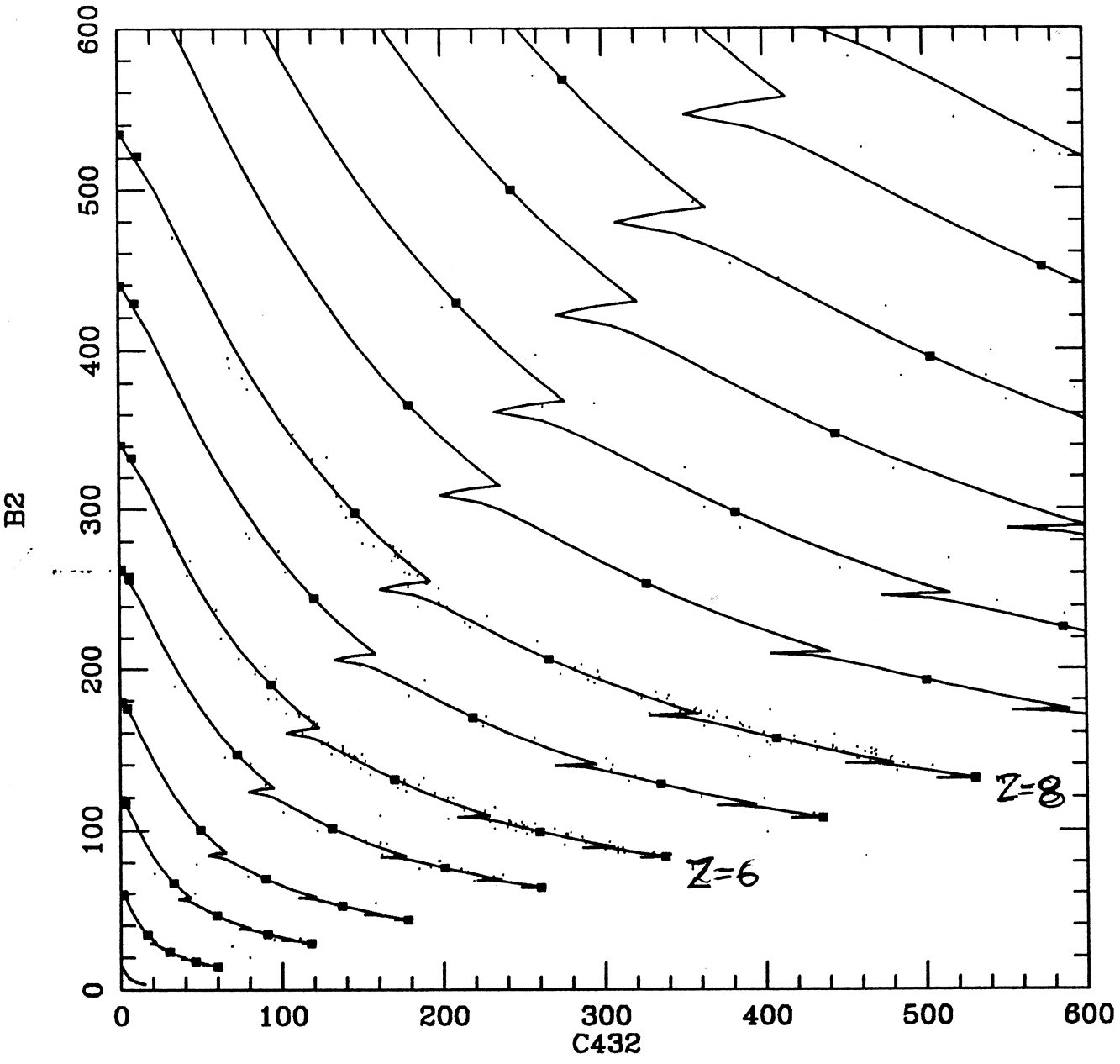

data file: s4v22b7_8.dat

evts read and selected: 475 397

|z2−z1| < 3.00*sigma, with sigma = 0.0550 + 0.0055*z

Energy bins from: ebinv22b.dat

simulation file: trv2h2.sim

Offset D1, D2, C:	0.00	0.00	0.00
FSMeV D1, D2, C:	2050.	4120.	16700.

Voyager-2,
HET - II
12/1/77 - 9/1/78
Low Gain events

Fig.40 The same as in Fig.37 for the energies deposited in B2 and C432 detector layers.

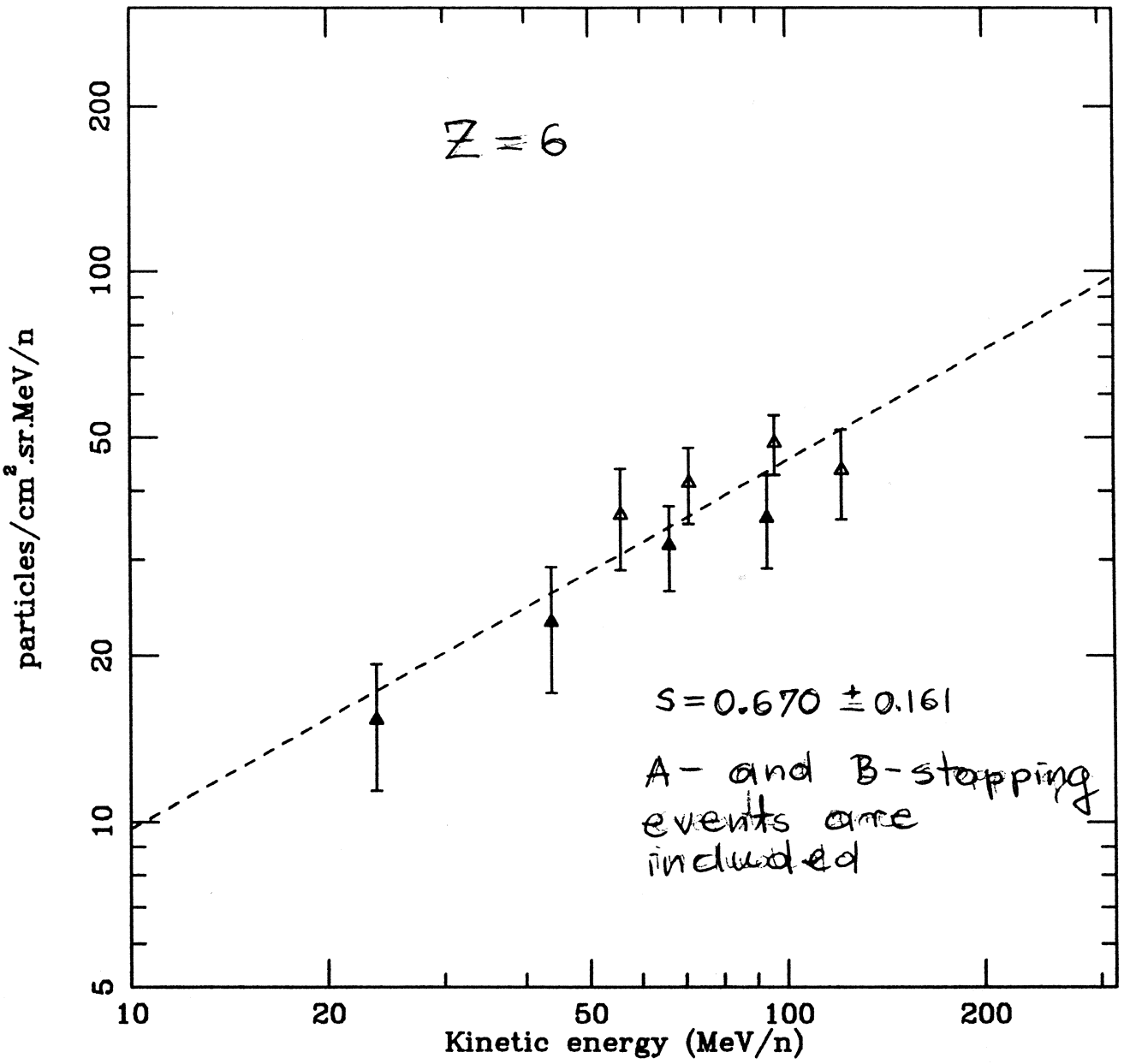

C : ▲ AS flv11a7_8.dat Δ BS flv11b7_8.dat

Fitted Galactic spectrum: $dJ/dE = 0.691E-01 * E^{0.670 +- 0.161}$

All fluxes times 30.0 TimeAS/TimeBS = 1.000

Fig.41 Flux versus energy (log-log scale) for Z = 6. The values of flux presented in figure are obtained from the analysis of both A- and B-stopping events registered by Voyager-1 detector HET-I in the time period of 12/01/77 - 4/01/78.

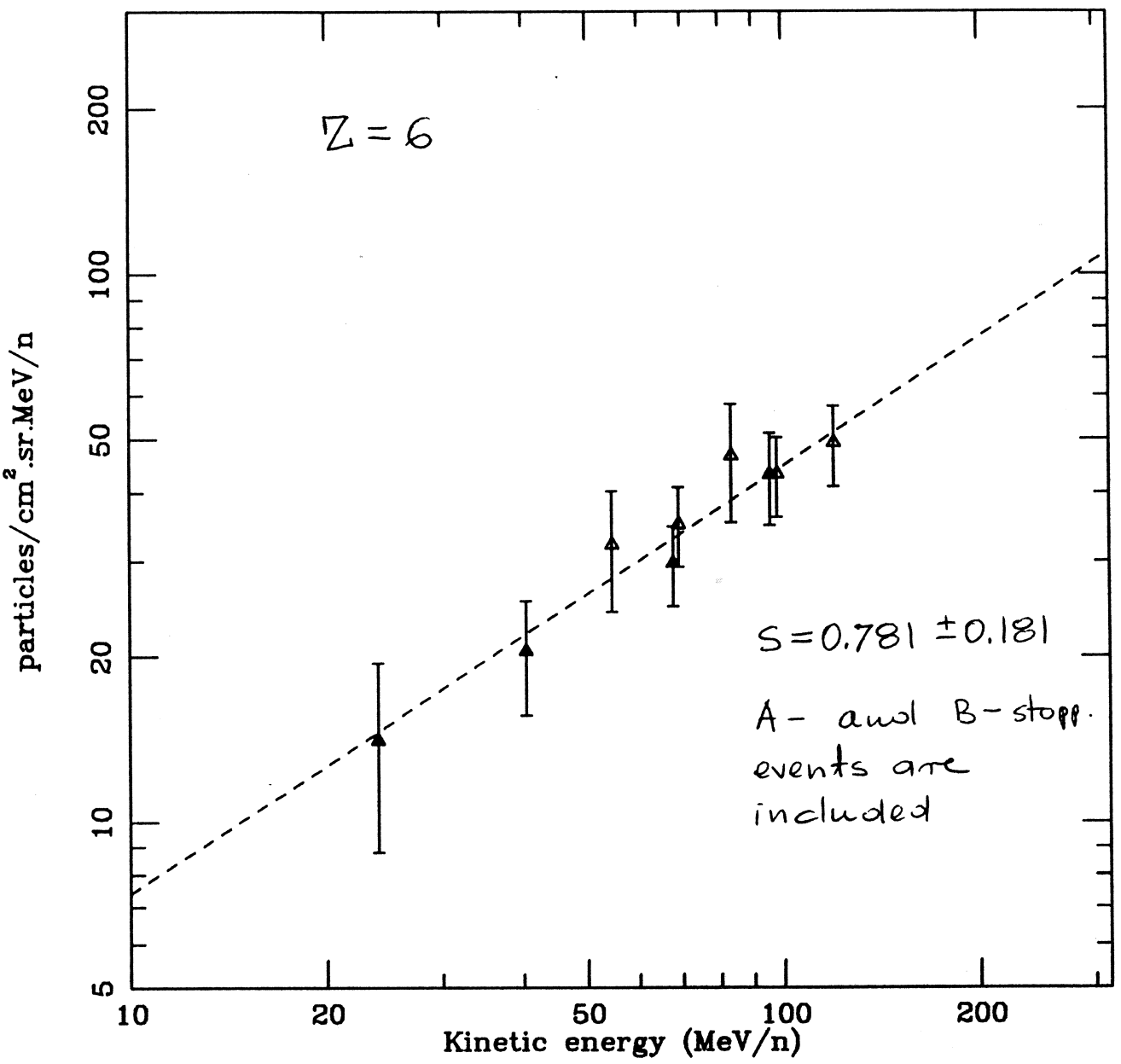

C : ▲ AS flv1asbin5.dat Δ BS flv1bsbin5.dat

Fitted Galactic spectrum: dJ/dE= 0.408E−01*E $^{0.781+-\ 0.181}$

All fluxes times 30.0 TimeAS/TimeBS = 1.000

Fig.42 Flux versus energy (log-log scale) for Z = 6. The values of flux presented in figure are obtained from the analysis of both A- and B-stopping events registered by Voyager-1 detector HET-II in the time period of 12/01/77 - 4/01/78.

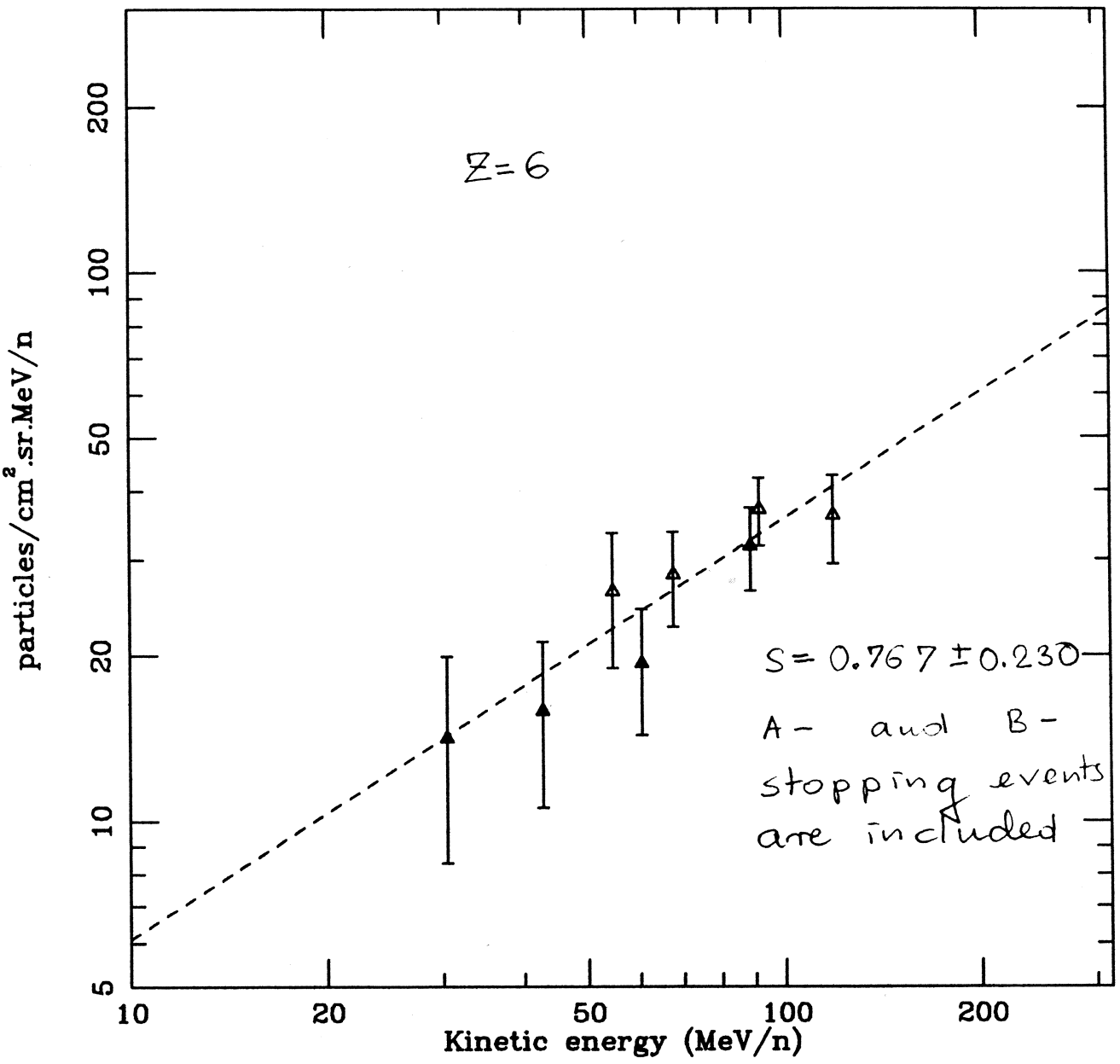

C : ▲ AS f6v21a7_8.dat Δ BS f6v21b7_8.dat

Fitted Galactic spectrum: $dJ/dE = 0.346E{-}01 * E^{0.767 +- 0.230}$

All fluxes times 30.0 TimeAS/TimeBS = 1.000

Fig.43 Flux versus energy (log-log scale) for Z = 6. The values of flux presented in figure are obtained from the analysis of both A- and B-stopping events registered by Voyager-2 detector HET-I in the time period of 12/01/77 - 4/01/78.

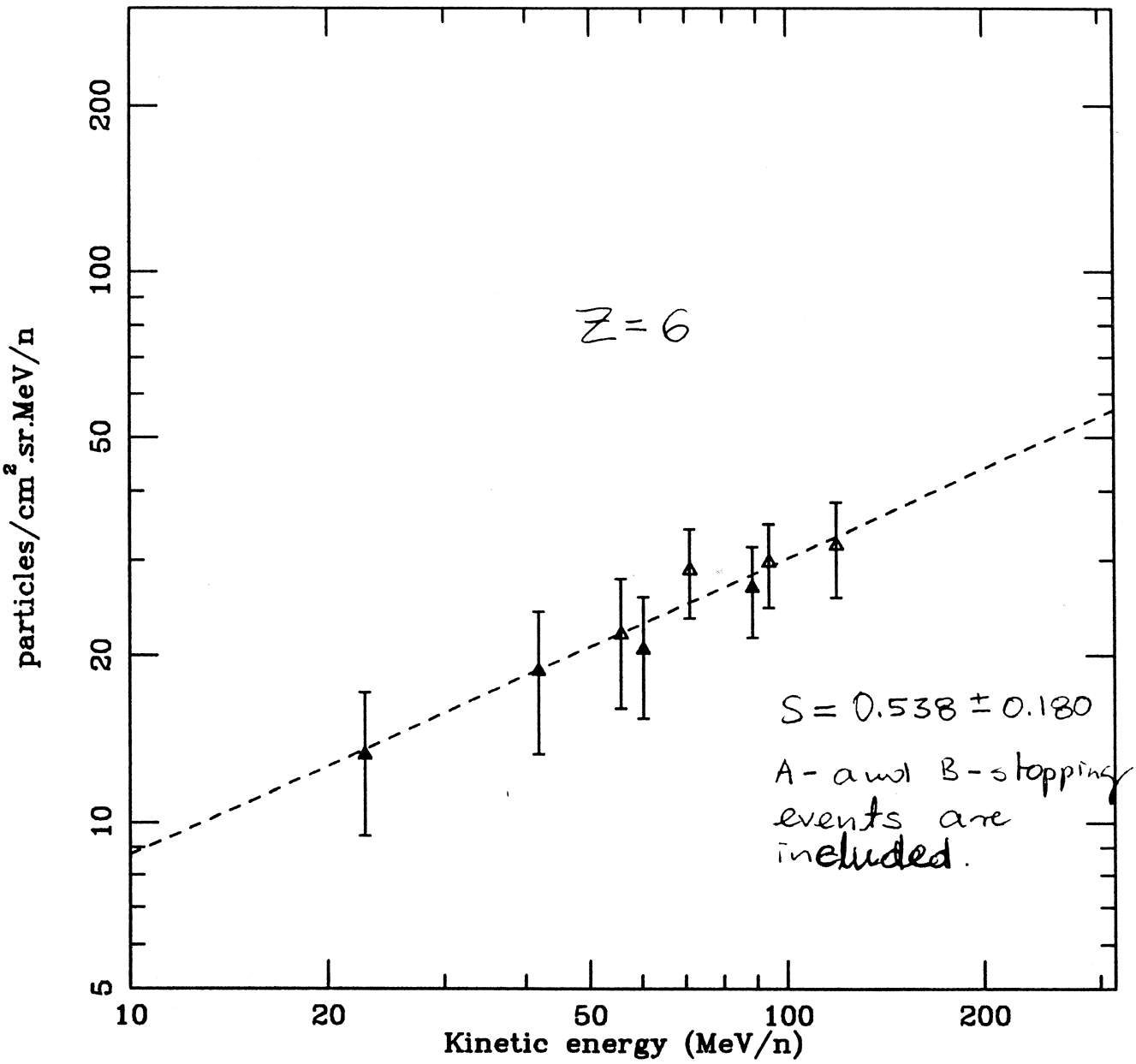

C : ▲ AS f6v22a7_8.dat Δ BS f6v22b7_8.dat

Fitted Galactic spectrum: dJ/dE= 0.844E−01*E $^{0.538+-\ 0.180}$

All fluxes times 30.0 TimeAS/TimeBS = 1.000

Fig.44 Flux versus energy (log-log scale) for Z = 6. The values of flux presented in figure are obtained from the analysis of both A- and B-stopping events registered by Voyager-2 detector HET-II in the time period of 12/01/77 - 4/01/78.

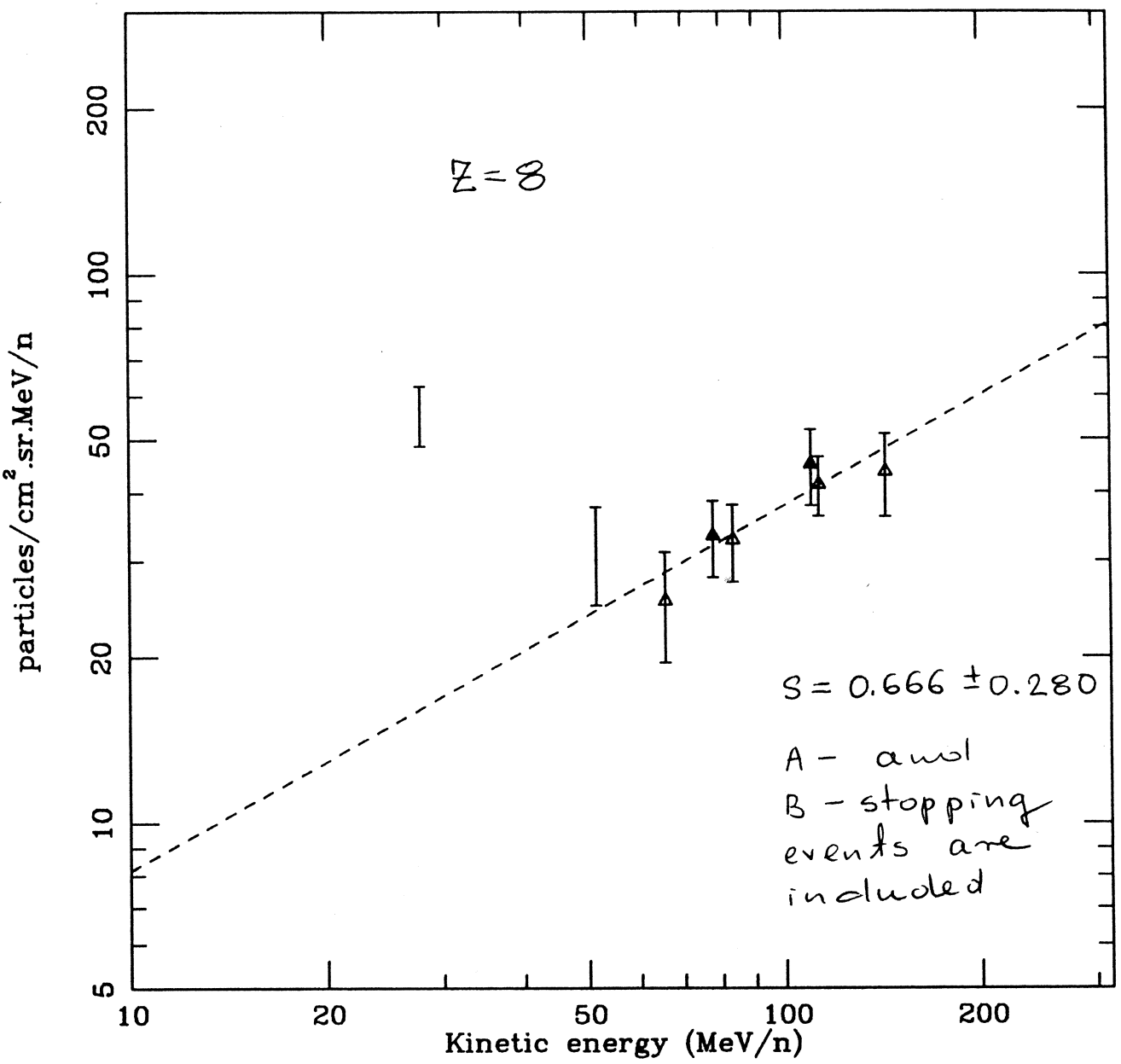

0 : ▲ AS flv11a7_8.dat Δ BS flv11b7_8.dat

Fitted Galactic spectrum: $dJ/dE = 0.587E-01 * E^{0.666 \pm 0.280}$

All fluxes times 30.0 TimeAS/TimeBS = 1.000

Fig.45 Flux versus energy (log-log scale) for Z = 8. The values of flux presented in figure are obtained from the analysis of both A- and B-stopping events registered by Voyager-1 detector HET-I in the time period of 12/01/77 - 4/01/78.

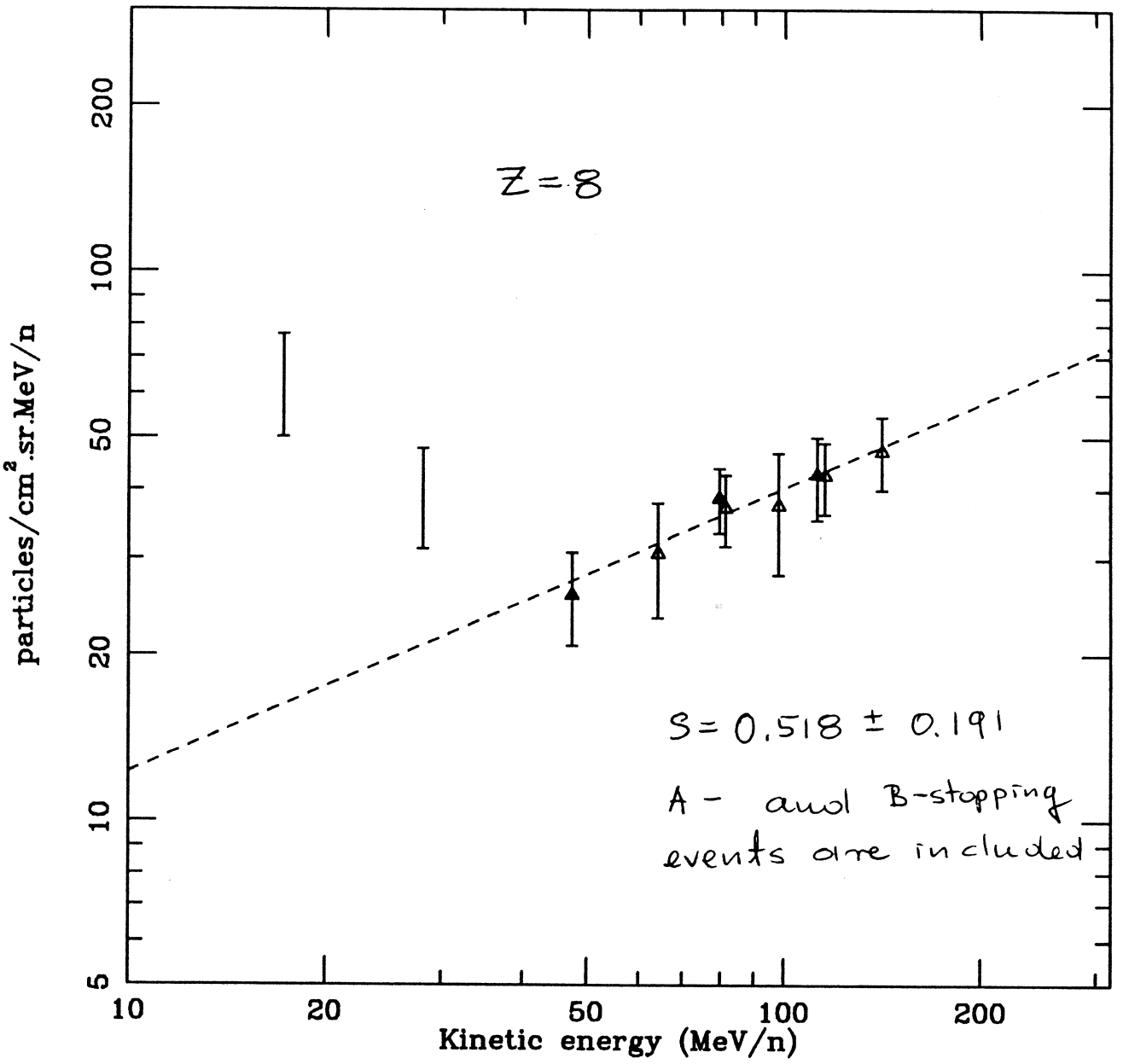

0 : ▲ AS flv1asbin5.dat Δ BS flv1bsbin5.dat

Fitted Galactic spectrum: dJ/dE= 0.124E+00*E $^{0.518+-\ 0.191}$

All fluxes times 30.0 TimeAS/TimeBS = 1.000

Fig.46 Flux versus energy (log-log scale) for Z = 8. The values of flux presented in figure are obtained from the analysis of both A- and B-stopping events registered by Voyager-1 detector HET-II in the time period of 12/01/77 - 4/01/78.

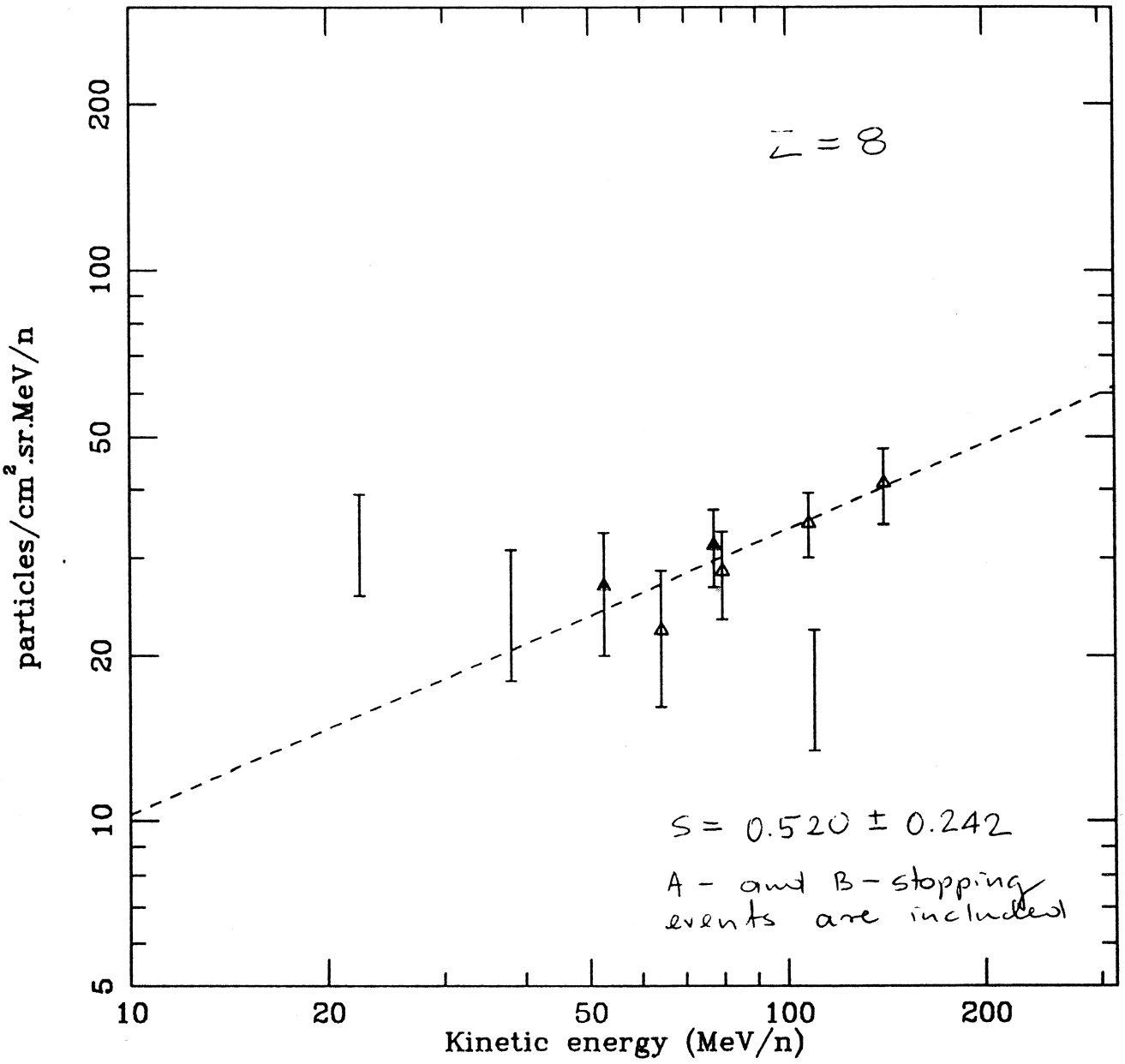

O : ▲ AS f8v21a7_8.dat Δ BS f8v21b7_8.dat

Fitted Galactic spectrum: $dJ/dE = 0.103E+00 * E^{0.520 \pm 0.242}$

All fluxes times 30.0 TimeAS/TimeBS = 1.000

Fig.47 Flux versus energy (log-log scale) for Z = 8. The values of flux presented in figure are obtained from the analysis of both A- and B-stopping events registered by Voyager-2 detector HET-I in the time period of 12/01/77 - 4/01/78.

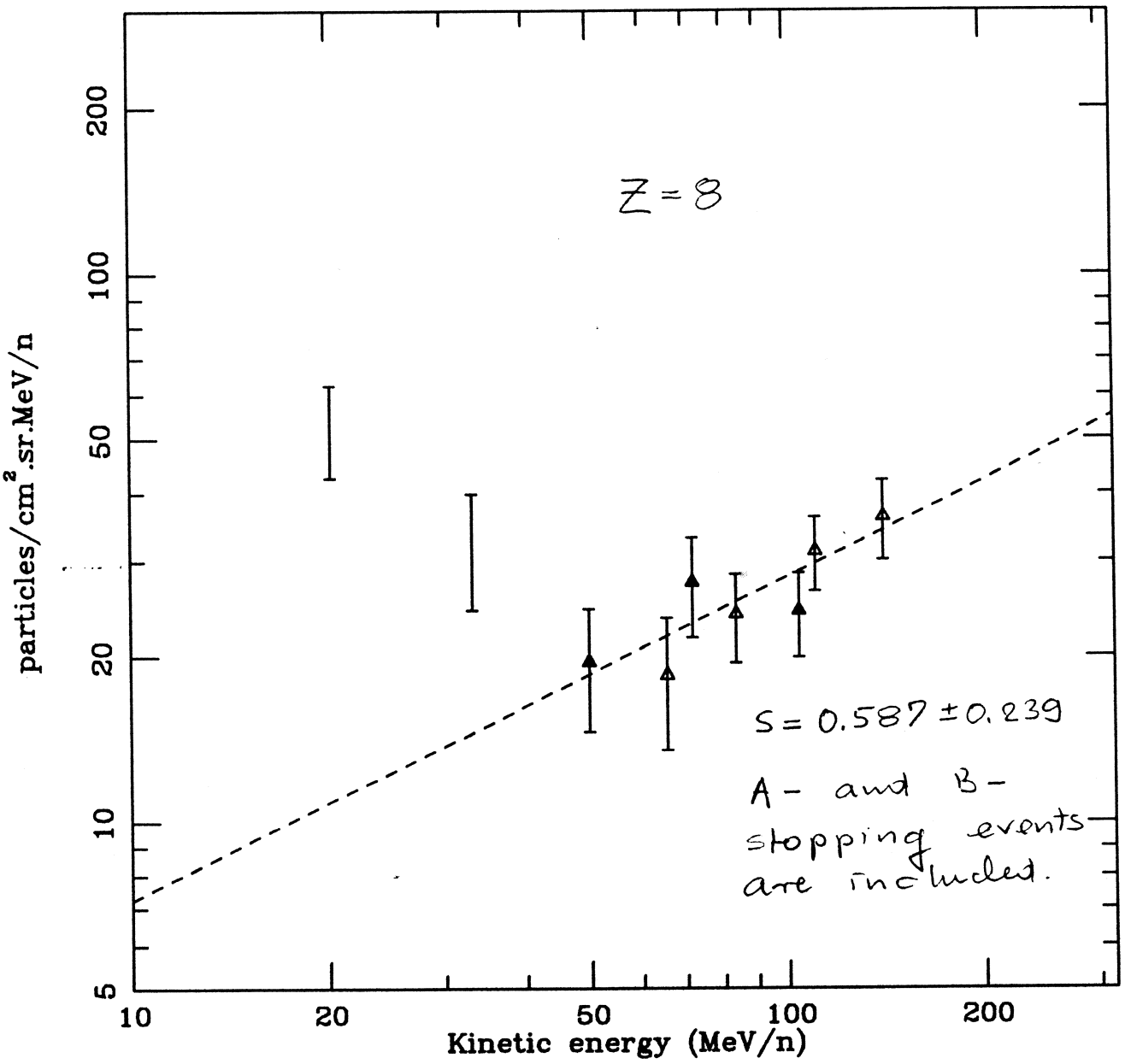

0 : ▲ AS f8v22a7_8.dat Δ BS f8v22b7_8.dat

Fitted Galactic spectrum: $dJ/dE = 0.623E-01 * E^{0.587 +- 0.239}$

All fluxes times 30.0 TimeAS/TimeBS = 1.000

Fig.48 Flux versus energy (log-log scale) for Z = 8. The values of flux presented in figure are obtained from the analysis of both A- and B-stopping events registered by Voyager-2 detector HET-II in the time period of 12/01/77 - 4/01/78.